Geotextiles and Geomembranes 53 (2025) 21–40

Contents lists available at ScienceDirect

Geotextiles and Geomembranes

journal homepage: www.elsevier.com/locate/geotexmem

Regular Paper

Unveiling the reinforcement benefits of innovative textured geogrids

Hasthi Venkateswarlu *, G. Madhavi Latha

Department of Civil Engineering, Indian Institute of Science, Bengaluru, 560012, India

ARTICLE INFO

Keywords:
Geosynthetics
Textured geogrid
3D printing
Interface coefficient
Aperture shape
PIV

ABSTRACT

The smooth surface texture of the commercially available geogrids limits the shear strength mobilization at the interfaces. This study presents the design, manufacturing, and interface performance evaluation of innovative textured geogrids. Geogrids with square, triangular, and hexagonal apertures with and without inherent surface texture were manufactured through additive manufacturing (3D printing) technique, using PLA (Poly Lactic Acid) filament. The texture includes elevated pins of 3 mm height at the junctions and inherent diamond pattern of 1 mm height on the ribs. The individual and combined effects of surface texture and aperture shape on the stress–displacement relationship, dilation angle, and the thickness of shear zone are quantified using large-scale direct shear tests and Particle Image Velocimetry (PIV) analysis. Results showed that the textured geogrid with hexagonal aperture has exhibited the maximum interface coefficient of 0.96 with sand followed by the geogrids with triangular and square apertures. Irrespective of the aperture shape, provision of the surface texture resulted in an overall increase of interface shear strength by more than 13%. Further, PIV analysis revealed that the shear zone is 25% thicker for textured geogrids of different aperture shapes, suggesting higher interlocking and passive resistance offered by their textured surfaces.

1. Introduction

The evolution of geosynthetics since their inception has led to a remarkable interest in incorporating them into numerous reinforced soil structures within the field of geotechnical engineering. Over the time, geosynthetics have become indispensable in various soil structures due to their ability to perform numerous functions and benefits, which include simplified construction, cost efficiency, exceptional performance under varying load conditions, and adaptability to a wide range of site conditions (Koerner, 2000; Shukla, 2004). Among the class of geosynthetics which are used to reinforce soils, geogrids are most popular and widely used. Because of their lighter and open structure, wide range of tensile strength and flexural stiffness, they found multiple applications in foundations, slopes, retaining walls, railroad embankments and pavements. Geogrids are manufactured in uniaxial, biaxial, triaxial, and multiaxial structures. The reinforcement benefits of a geogrid are majorly governed by its tensile strength and interface shear strength with soil. The geometric shape of the geogrid, its structure, opening shape and size are continuously evolving to suit various applications (Prakash et al., 2023; Ziegler, 2017; Venkateswarlu and Hegde 2019).

The shear behavior of interfaces between the soil and geosynthetics is commonly measured through modified direct shear tests (Lashkari and Jamali, 2021; Zeng et al., 2022; Liu et al., 2022; Maghool et al., 2020; Naeini et al., 2013; Razeghi and Ensani, 2023; Araújo et al., 2022; Palmeira and Antunes, 2010). Literature reveals that the interface shear resistance is affected by several factors, most importantly, shape and size of the soil particles, applied normal stress, density of soil and moisture content (Brown et al., 2007; Pitanga et al., 2009; Miyata and Bathurst, 2012; Vieira and Pereira, 2016; Mirzaalimohammadi et al., 2019; Stoltz et al., 2020; Ying et al., 2021; Ding et al., 2022). For a longer time since their inception, aperture shape of the geogrid was mostly kept as square in case of biaxial geogrids and near rectangular in case of uniaxial geogrids. Recently, the aperture shape of the geogrid has received a lot of attention, and a reasonable number of studies explored the effect of geometry of geogrid on the shear strength response of geogrid-soil interfaces. Through large-scale direct shear tests on interfaces between construction demolition waste and geogrid, Arulrajah et al. (2014) showed that triaxial geogrids exhibit higher shear resistance compared to biaxial geogrids. Ferreira et al. (2015) reported that the biaxial geogrid provides superior interface shear strength in comparison with the uniaxial geogrid. Direct shear tests conducted by Zhang et al. (2021a,b) reveal that the triaxial geogrid exhibits greater interlocking effect with the soil particles compared to the biaxial geogrid. More recently, researchers and practitioners are also using hexagonal geogrids

* Corresponding author.
E-mail addresses: hvenkateswar@iisc.ac.in, venki.hasthi@gmail.com (H. Venkateswarlu), madhavi@iisc.ac.in (G.M. Latha).

https://doi.org/10.1016/j.geotexmem.2024.08.008
Received 15 April 2024; Received in revised form 21 August 2024; Accepted 30 August 2024
Available online 9 September 2024

(Górszczyk and Malicki, 2023). Some of the innovative bio-inspired geogrids which are under evolution include spider web shaped geogrids (Liu, 2020).

Many studies on interface shear response of geogrids and sands pointed out the significance of aperture size on the interface shear strength. Vangla and Gali (2016) suggested an optimum asperity ratio (a_s/D_{50}, where, a_s is the geogrid aperture size and D_{50} is the average particle size of the sand) of 1.0 for the efficient entrapment of sand particles within the apertures and to achieve the highest interfacial shear strength. To establish the efficient load transfer, Derksen et al. (2021) recommended an optimum aperture ratio as 4.2 times the mean particle size of sand. Venkateswarlu et al. (2023a) demonstrated the benefits of triangular geogrid in achieving higher interface shear strength over circular and square geogrids. The optimum limit of aperture ratio to derive maximum benefits from geogrid was reported as 2–11.29.

One of the new innovations on the geometric evolution of geogrids is in the form of 3D reinforcing elements. These elements were developed by raising the height of the transverse ribs without changing the height of the longitudinal ribs to attain higher passive resistance. Makkar et al. (2019) studied the interaction behavior of 3D reinforcement elements of rectangular and triangular shapes with sand and showed that rectangular elements exhibited higher interface coefficient compared to triangular elements. Mosallanezhad et al. (2016) demonstrated the effectiveness of geogrid-anchor (GA) reinforcement over the planar geogrid in improving the interface shear strength. The shear strength measured for GA-sand interface was 50% higher than the shear strength measured for planar geogrid-sand interface.

Though considerable amount of research is published in this area, geogrids of newer shapes are not commercially available. They are usually manufactured in a small scale, through manual fabrication techniques like strapping, welding, and gluing. However, manual fabrication techniques result in nonhomogeneous structures with significant variation in physical and mechanical properties in different directions (Liu et al., 2016; Wu et al., 2020). Rapidly evolving additive manufacturing technology (referred to as 3D printing) is an efficient approach for developing geogrids of required geometry at a small scale with reasonable homogeneity in material properties (Latha et al., 2024). The 3D printing technique has been successfully employed by many researchers to manufacture geosynthetics using polymers at a lab scale (Chalmovsky et al., 2020; Fowmes et al., 2017). Stathas et al. (2017) utilized 3D printing to create miniature geogrid models and suggested that these models were suitable for application in laboratory model tests. Arab et al. (2020) highlighted the effectiveness of printed hexagonal-shaped geogrid in improving the bearing capacity of reinforced soil beds. However, large-scale mass production of geogrids using 3D printing technique is currently not possible. With the control on geometry, properties and accuracy, 3D printing technology is expected to soon evolve and support the mass production. The current study used 3D printing method to manufacture geogrids of distinct shapes and surface texture and used them in interface shear tests.

The availability of new generation computational facilities nudged the researchers towards the use of digital methods to understand the internal mechanisms at micro scale and explain the macro level manifestations in experiments. Digital Image Correlation (DIC) technique has become popular in geotechnical engineering to derive the clues for macro scale response from the micro scale perspective. One subset of DIC technique is Particle Image Velocimetry (PIV), which helps in understanding the deformation behavior of sand during physical modelling (White et al., 2003; Escobar et al., 2021; Peerun et al., 2019; Stanier et al., 2016). PIV can also be applied for quantifying the strain fields in geosynthetics during tension tests (Jayalath and Gallage, 2021; Mishra et al., 2016). Further, using PIV approach, several researchers have quantified the thickness of shear zone during pull-out and interface shear tests (Abdi and Mirzaeifar, 2017; Ferreira and Zornberg, 2015; Giang et al., 2010; Zhou et al., 2012; Bathurst and Ezzein, 2015).

Though the geometry and structure of the geogrid have undergone several changes over the years to perform the reinforcement function effectively, a little or no consideration has been given to the texture of the geogrid surface, which is very important in maintaining good bond strength with soils. In this context, the current study presents a new class of novel geogrids, which have texture on their surface and the effectiveness of these geogrids in improving the overall interface shear strength when bonding with sand is investigated for geogrids of different aperture shapes. Textured geogrids of different apertures shapes were developed using 3D printed technique. A series of large-scale direct shear tests were conducted to explore the effect of surface texture on the shear stress response of various geogrid-sand interfaces. Further, particle dynamics during interface shear interactions were captured through PIV analysis. The study aims at demonstrating the multiple benefits of surface texture of geogrids by means of interface shear tests, explaining the internal mechanisms using PIV analysis and quantifying the contribution of surface texture to the interface shear strength through comparisons.

2. Experimental investigation

2.1. Test materials

Grain size distribution of the river sand used in the direct shear tests is shown in Fig. 1. The sand has mean particle size of 0.7 mm and it is classified as poorly graded sand (SP), as per the Unified Soil Classification System (ASTM D-2487, 2011). Table 1 summarizes the properties of the sand. The procedures outlined in ASTM D-4253 (2016) and ASTM D-4254 (2016) were used to calculate the maximum and minimum dry unit weights of the sand, respectively. Further, large-scale direct shear experiments were performed to determine the shear strength parameters of sand. These direct shear tests were conducted at different normal stresses of 40 kPa, 80 kPa, and 120 kPa, while maintaining a uniform relative density of 80%. Fig. 2 presents the failure envelope of sand obtained from direct shear tests. The cohesion and internal friction angle of the sand were determined as 0.8 kPa and 37°, respectively.

Poly Lactic Acid (PLA) filament was utilized for 3D printing the geogrids. It is a bio-based polymer obtained by fermenting plant starches, such as corn, sugarcane, and maize. Geogrids of different aperture shapes with and without surface texture were customized and manufactured in the laboratory, using a Fused Deposition Modeling (FDM) type 3D printer of Pratham Make 3D 5.0 make, with a printing accuracy of 0.1 mm. In the FDM printing technique, the required object is formed by melting a continuous thermoplastic filament and fusing it

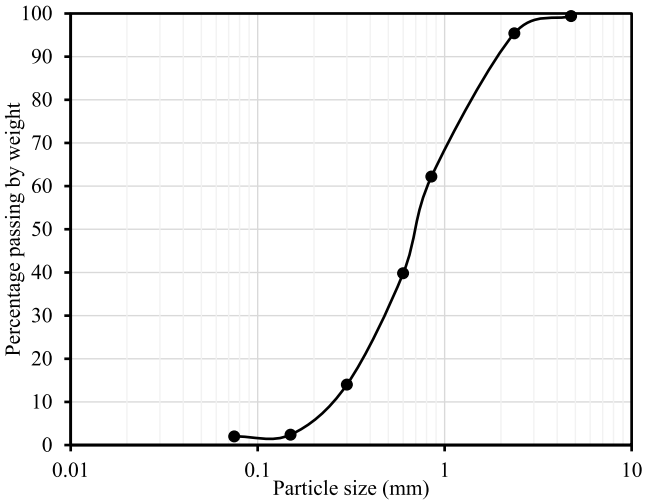

Fig. 1. Particle size distribution of sand.

Table 1
Properties of sand.

Property	Value
Specific gravity (G)	2.61
Mean particle diameter (D_{50}), mm	0.7
Fines content (particle size <75μ), %	2
Coefficient of uniformity, C_u	3.2
Coefficient of curvature, C_c	1.15
Maximum void ratio, e_{max}	0.64
Minimum void ratio, e_{min}	0.39
Maximum dry unit weight (γ_{max}), kN/m^3	18.4
Minimum dry unit weight (γ_{min}), kN/m^3	15.6

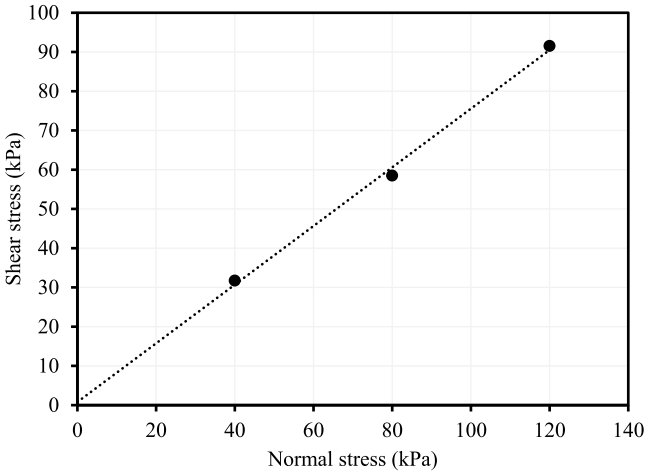

Fig. 2. Failure envelope of sand obtained from direct shear test.

together in successive layers. The detailed specifications, components, and the printing methodology of the FDM based 3D printer used in this study can be found in our earlier studies (Venkateswarlu et al., 2023a, 2023b; Latha et al., 2024).

Geogrids with square, triangular, and hexagonal apertures as shown in Fig. 3 were printed by strictly adhering to the specific printing parameters. In this study, a printing speed of 40 mm/s was chosen based on numerous trials of printing to maintain consistent layering without any peeling issues. The preheat temperature for melting the PLA material and the bed temperature were 220 °C and 70 °C, respectively. Maintaining the bed temperature results in significant advantages for 3D printing of geogrids. Firstly, it improves the bed adhesion. It was noticed that by maintaining the temperature of printing bed at 70 °C, which is considerably higher compared to the ambient temperature, the initial layer of extruded filament stays soft for a longer time, promoting better first-layer adhesion. Moreover, this temperature contributes to enhanced print quality by minimizing the warping issues. Once the heated bed is turned off, the temperature decreases rapidly, which aids in the easy removal of the finished parts. Further, a 100% internal density was used for printing the geogrids to achieve optimal material strength. Different 3D printed geogrids and their corresponding designations are shown in Fig. 4. SG, TG, and HG indicate the geogrids with square, triangular, and hexagonal apertures, respectively. For convenience, the geogrids with square, triangular and hexagonal apertures will be denoted as square geogrids, triangular geogrids, and hexagonal geogrids, respectively. The letter symbol P added at the end represents the geogrids with pins at the junction and the letter symbol T at the end represents textured geogrids. For example, SGP represents a non-textured geogrid with square apertures and pins at the junction, and SGPT represents a textured geogrid with square apertures and pins at the junction. This nomenclature is followed for all geogrids shown in Fig. 4.

The aperture area of different geogrids was maintained the same (approximately 1090 mm^2) in different shapes to derive better comparisons. Fig. 4 highlights the dimensions of each side for various aperture shapes. The rib width was maintained as 5 mm in both longitudinal and transverse directions. The thickness of all geogrids was

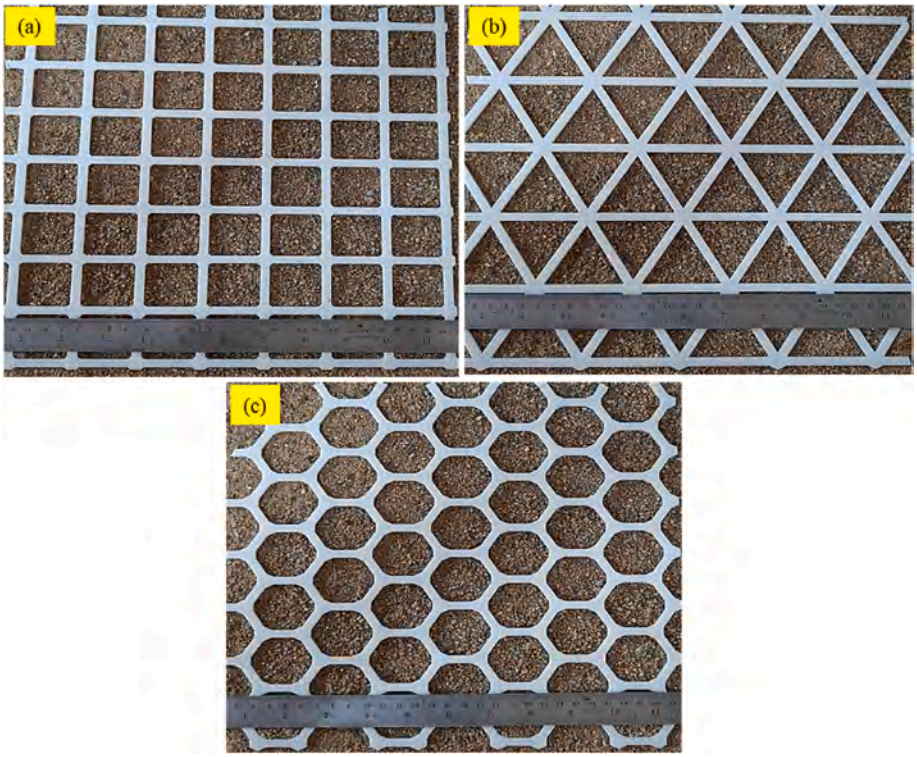

Fig. 3. Geogrids of different aperture shapes: (a) square; (b) triangular; and (c) hexagonal.

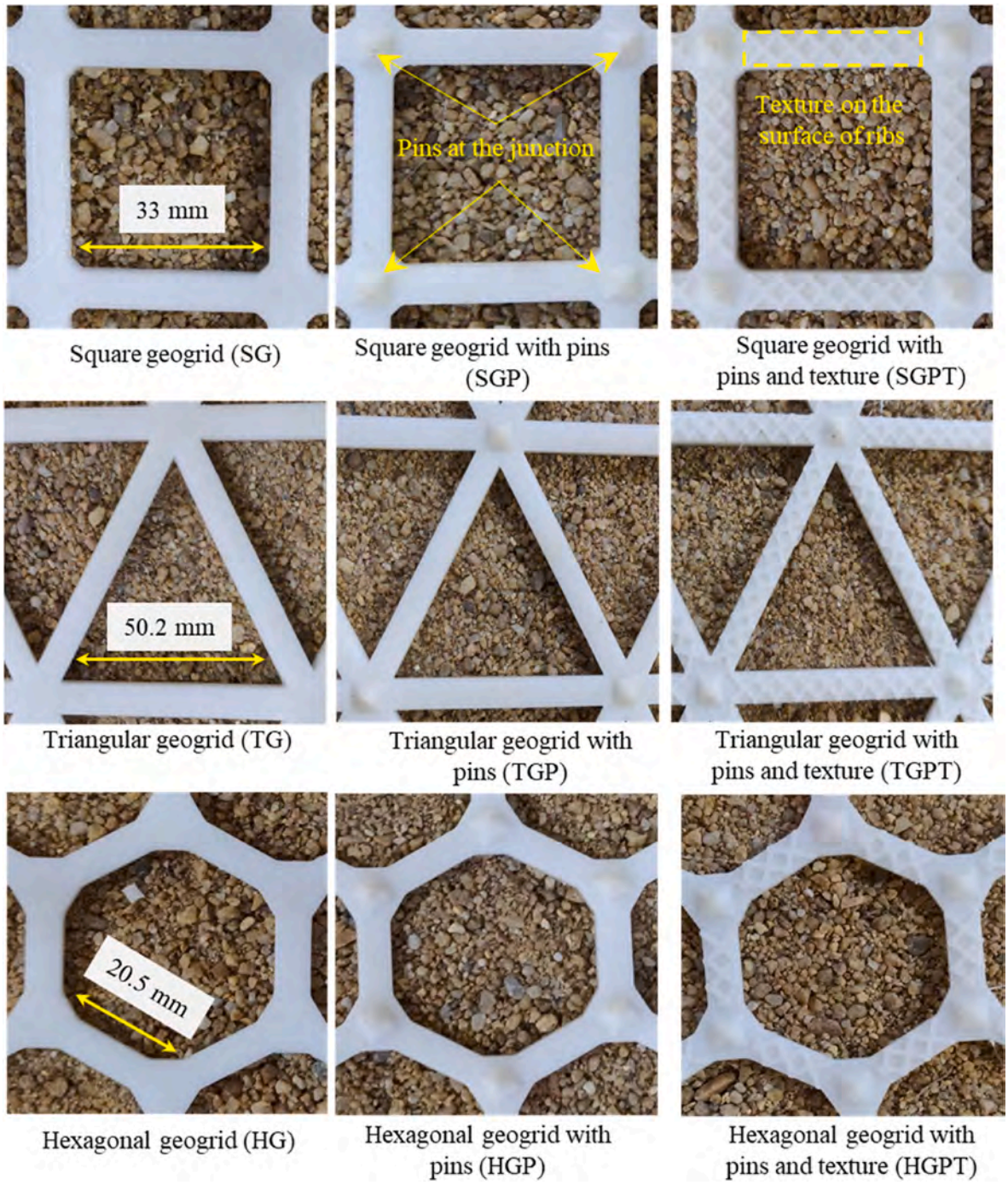

Fig. 4. Different configurations of geogrids.

uniformly kept as 3 mm, with textured geogrids having an additional thickness of 1 mm at the elevated diamond pattern. The ratio between the texture height on the surface of the geogrid rib to the D_{50} of the sand is 1.43, and the ratio between the height of the junction pin to the D_{50} of the sand is 4.3. The anchor pins were designed to a pyramid shape with a base area of 36 mm^2 and height of 3 mm. The pyramid-shaped pins offer the advantage of providing resistance against the movement of sand particles from four different faces while shearing. Texture was created only on the top surface of the rib. In FDM 3D printing process, objects are printed on a flat glass surface, referred to as touch bed. Therefore, the printed objects will invariably have a flat surface at the bottom. A close-up view of the texture in different configurations is shown in Fig. 5.

After printing the geogrids, their physical and mechanical properties were determined and listed in Table 2. The mass per unit area of different geogrids was estimated from the quantity of raw material utilized in printing. Although the aperture area was almost the same for all geogrids, triangular geogrids exhibited slightly higher mass per unit area, followed by square geogrids, and hexagonal geogrids in all configurations. This minor variation caused by the change in structure of the geogrid can be attributed to the changes in layering. Interestingly, at a specific aperture shape, the difference between the mass per unit area values of a geogrid with pins and texture and without texture is marginal. Adding texture to the surface did not change the mass per unit area significantly, and hence the cost of textured geogrids is not substantially greater in comparison with the non-textured geogrids of same configuration.

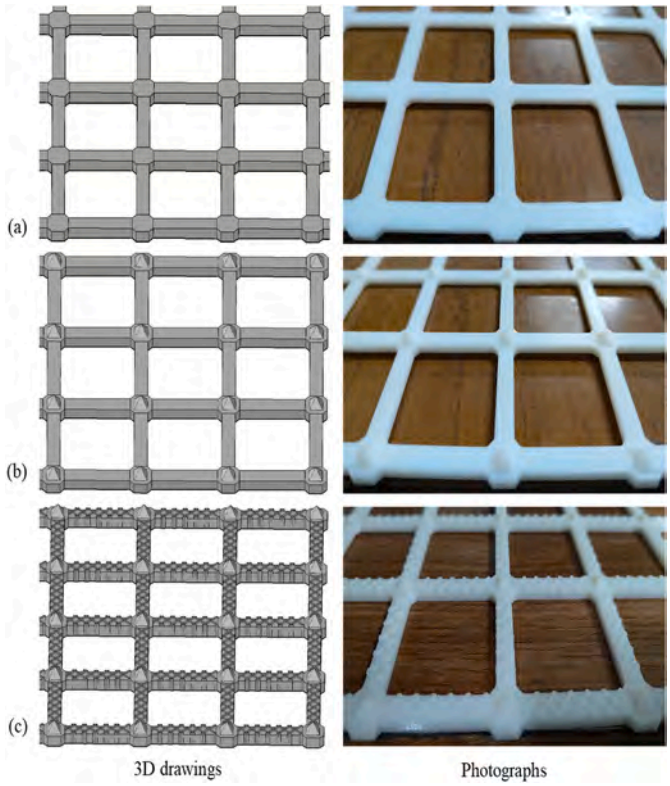

Fig. 5. Different configurations of geogrids: (a) geogrid without pins and surface texture; (b) geogrid with only pins at the junctions; and (c) geogrid with pins and surface texture.

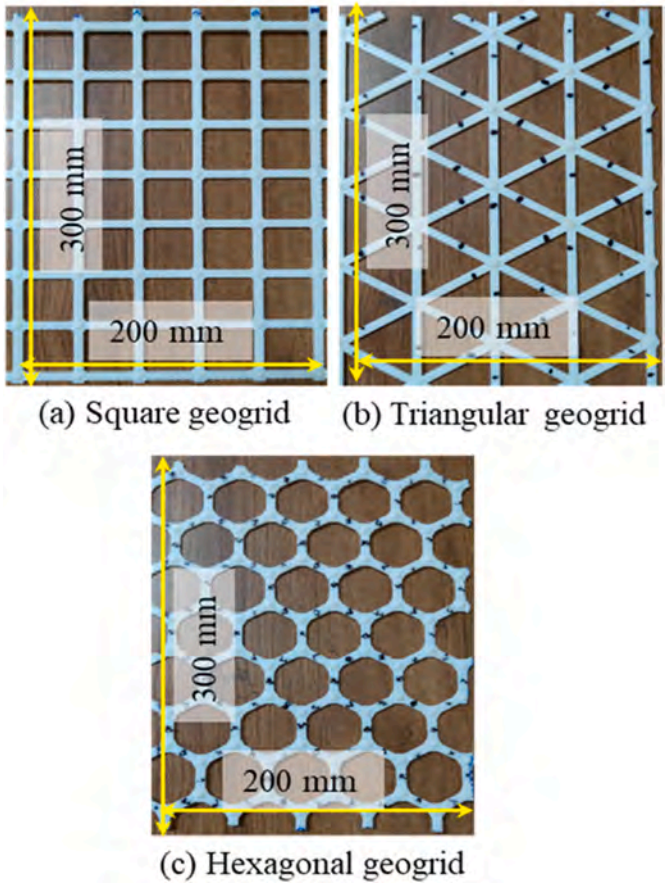

Fig. 6. Dimensions of different geogrid specimens used in tension test.

Table 2
Properties of geogrids of different configurations.

Geogrid configuration	Mass per unit area (g/m^2)	Mechanical parameters		
		Peak tensile load (kN/m)	Failure strain (%)	Secant modulus at 2% strain (kN/m)
SG	1088	19.20	4.40	495
SGP	1111	20.16	5.06	499
SGPT	1130	21.58	5.40	504
TG	1122	21.33	5.12	551
TGP	1125	22.89	5.73	558
TGPT	1148	23.55	6.02	562
HG	1064	24.97	5.38	777
HGP	1096	26.72	5.87	784
HGPT	1121	27.94	6.07	789

The tensile behaviour of different geogrids was studied by performing wide width tension tests using a universal testing machine, following the guidelines of ASTM D-6637 (2011). The specimens used in tension tests were 200 mm wide and 300 mm long as shown in Fig. 6. The specimen dimensions were chosen as per the standard multi-rib tensile test method specified in ASTM D-6637 (2011). This method specifies that the geogrid specimens for tensile tests must have a minimum 200 mm width and 300 mm length and contain at least five ribs along the width and three junctions along the length. The specimens used in the current study conform to these specifications. Several earlier studies on geogrids of different aperture shapes have also used specimens of 200 mm width in tension tests (Zhang et al., 2021a,b; Dong et al., 2011). The results of tension test are shown in Fig. 7. Based on the tensile response, failure strain and secant modulus were calculated and listed in Table 2. The highest tensile strength of 24.97 kN/m was measured for the hexagonal geogrid (HG), followed by the triangular geogrid (TG), and square geogrid (SG). Though tensile strength of the geogrids is primarily a material property, the geometric arrangement of a geogrid can significantly influence its effective tensile strength when considered as a structural system. In the case of hexagonal geogrids, six ribs offer tensile resistance in six directions. Whereas geogrids with triangular apertures offer triaxial resistance and in case of geogrids with square apertures, the resistance is mainly derived in two orthogonal directions. Therefore, the geogrid with hexagonal aperture is more efficient to distribute the uniaxial tension from different directions than the geogrid with triangular and square apertures. As a result, hexagonal geogrid exhibited higher tensile strength than triangular and square geogrids. The tensile strength was found to increase with the provision of pins at the junctions and was maximum for geogrids with pins and surface texture. Similarly, provision of surface texture and pins at the junctions resulted in the increase in the failure strain, irrespective of the aperture shape.

Provision of pins at the junctions of the geogrid offers multiple benefits, which include enhancement of the junction integrity, increase in resistance to vertical deformation, anchoring effect with the soil in contact and providing a stable geometric structure to the geogrid, thus increasing the tensile load capacity of the geogrids. Further, addition of surface texture to the ribs makes them stronger under tension, apart from helping in increased interlocking of particles into the texture. The variation in secant modulus was found to be marginal for the geogrids of same aperture shape, with and without surface texture.

3. Methodology

Through interface direct shear tests coupled with PIV analysis, the behavior of textured geogrid-sand interfaces is comprehensively investigated. This integrated approach not only provides detailed insights into the mechanical response of interfaces but also provides clues for optimized geogrid design for their application in reinforced soil projects.

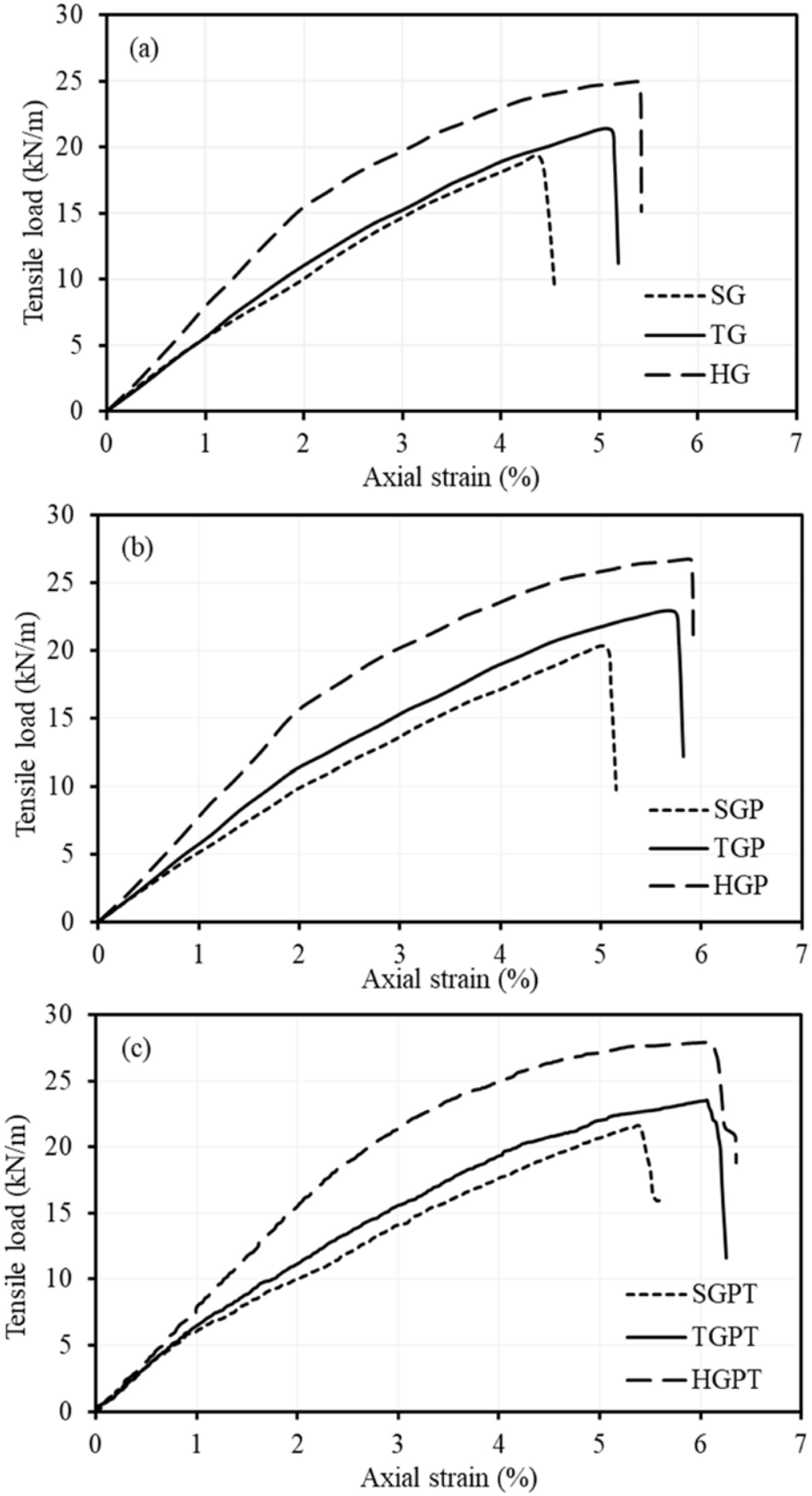

Fig. 7. Tensile response of geogrids with different aperture shapes: (a) without pins and surface texture; (b) with only pins at junctions; and (c) with pins and surface texture.

The following subsections provide a detailed discussion on the methodologies adopted for testing.

3.1. Direct shear tests

To explore the influence of surface texture on the shear behavior of geogrid-sand interfaces, interface direct shear tests were conducted. The photograph of the test setup is shown in Fig. 8. The setup consists of a shear box of 300 mm (length) × 300 mm (width) × 200 mm (depth), divided into fixed upper box and movable bottom box. These box dimensions conform to the specifications given in ASTM D-5321 (2002) to avoid the dimensional scaling effects on the shear response. The geogrid reinforcement was positioned at the top of the movable lower box to facilitate better interaction with the sand, as suggested by Liu et al. (2009), and Arulrajah et al. (2014). During the tests, the interface was sheared at a controlled displacement rate of 1.25 mm/min. The variation of shear load and horizontal displacement was thoroughly monitored using a load cell and a horizontal LVDT (Linear Variable Differential Transformer), respectively. Using shear load, the shear stress was calculated by dividing it with the area of contact between the geogrid surface and the sand.

Two series of direct shear tests were conducted. In series I, tests were conducted on sand without reinforcement to quantify its shear strength parameters. In the test series II, shear tests were performed on different geogrid-sand interfaces with various geogrid aperture shapes and surface texture configurations. The details corresponding to each series of experiments are summarized in Table 3. Relative density of 80% was maintained in both the series of tests to represent the dense compaction of sand in reinforced earth structures. In each series of the interface shear tests, one shear test was repeated to confirm the reproducibility of results. In total, 40 large-scale interface shear tests, including repetitive tests were performed.

3.2. PIV analysis

Though the results of interface shear tests are useful for quantifying the shear strength parameters of various geogrid-sand interfaces, this information is not adequate to understand and visualize the particle movement and internal mechanisms involved in the shearing process. To understand and analyse these micro scale internal processes, Particle Image Velocimetry (PIV) analysis was carried out. High-definition videos of the shearing plane with the field of view extending to 60 mm on both sides of the plane were captured continuously using a high-definition Canon EOS 450D camera. Subsequently, the videos were converted into a series of images captured at specific time intervals employing the PIV-lab tool and analysed in MATLAB. The images that were ripped have the quality of 72 dpi and size of 4272 × 2848 pixels. PIV is an optical image correlation technique that analyses the velocity fields in a sequence of images through an autocorrelation function to describe and quantify the movement of objects. By comparing these images, displacement vectors are generated to understand the movement of particles with time (Grognet, 2011; White and Take, 2002; Fukuoka et al., 2007). This vector illustration aids in visualizing the displacement distributions near the interface and distinguishing interlocking response of different textured geogrid-sand interfaces. The displacement fields and vector intensities are correlated to the microscopic shear mechanisms like sliding and interlocking, which are further used to explain the macroscopic shear response. Thus, a comprehensive understanding of the geogrid-sand interface shear behavior at multiple scales is obtained.

Table 3
Details of interface shear tests.

Interface type	Aperture shape of the geogrid	Geogrid designation	Normal stress (kPa)	Total tests
Sand-Sand	–	–	40, 80, 120	3
Geogrid-Sand	Square	SG, SGP, SGPT	40, 80, 120	9
	Triangular	TG, TGP, TGPT	40, 80, 120	9
	Hexagonal	HG, HGP, HGPT	40, 80, 120	9

4. Results and analysis

Fig. 9 presents the shear stress-displacement response of sand-square geogrid interfaces with different surface texture configurations. The letter "R" in Fig. 9 denotes the response obtained from repeated shear tests. The close match between repeated tests confirms the

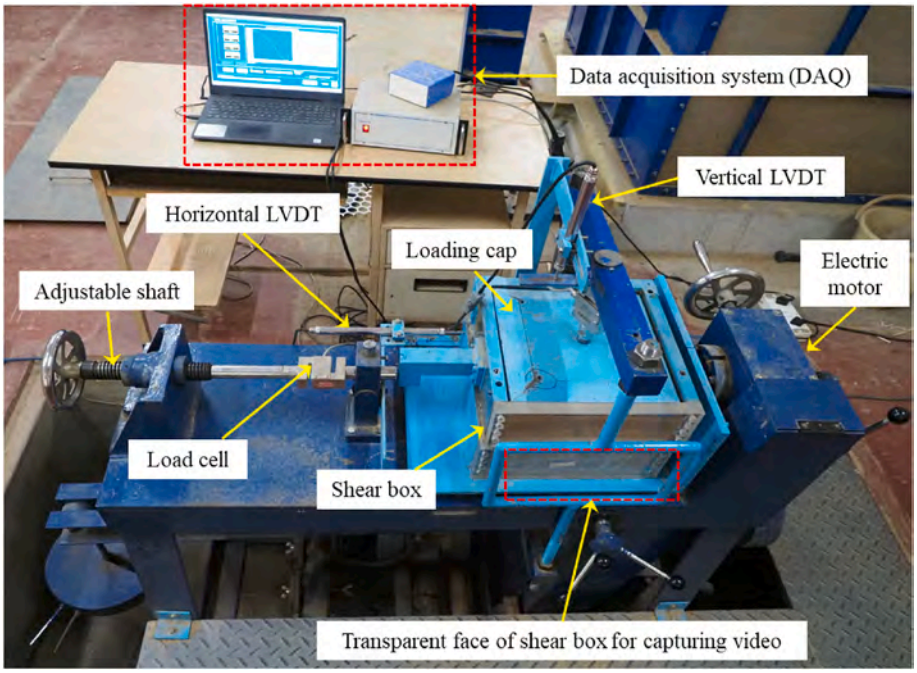

Fig. 8. Large scale direct shear test setup.

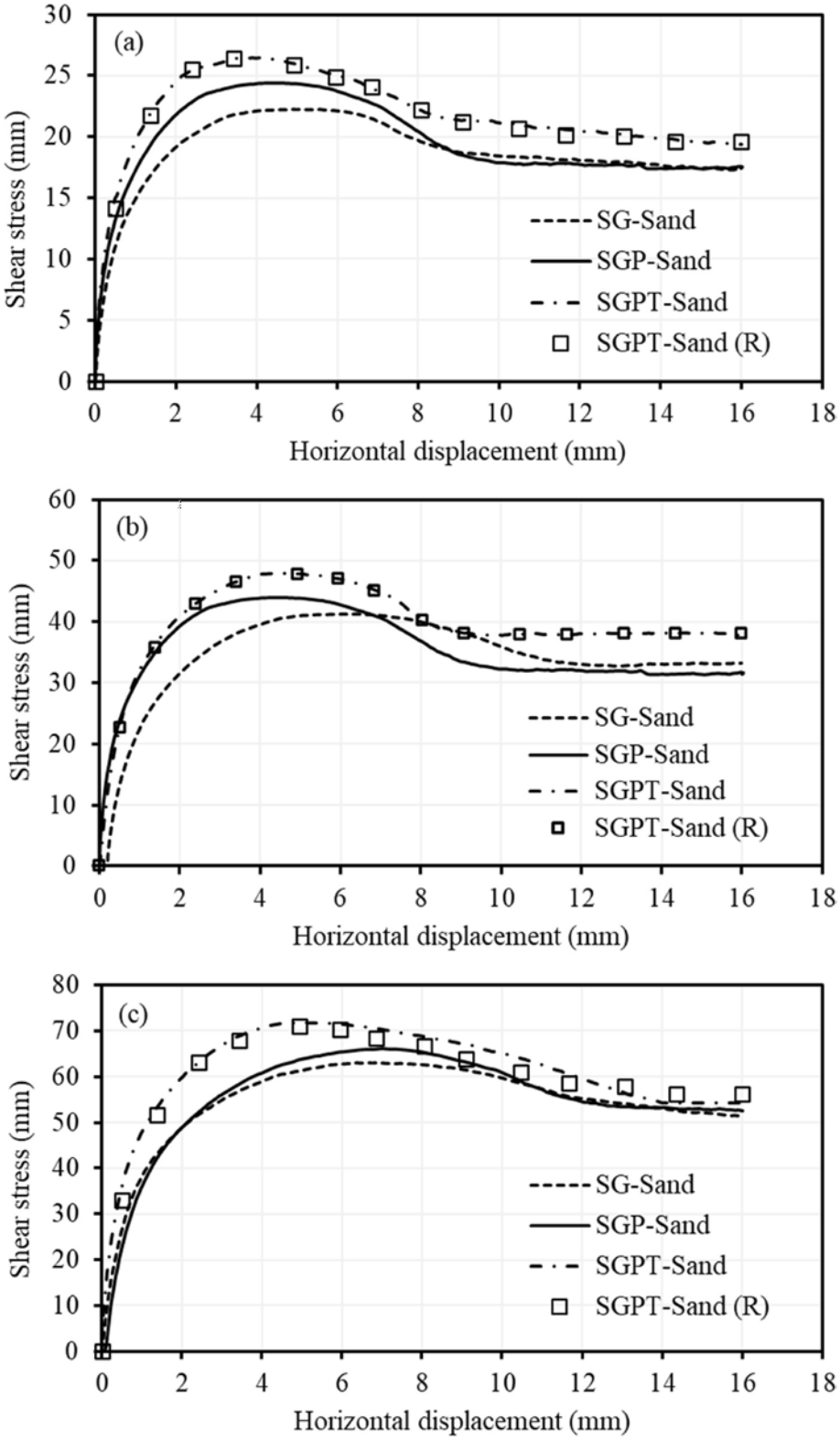

Fig. 9. Shear stress variation of square geogrid-sand interface with different texture configurations: (a) 40 kPa; (b) 80 kPa; and (c) 120 kPa.

reproducibility of test results, providing confidence about the consistency of testing procedures and uniformity in geogrid manufacturing. Among the three different square geogrid-sand interfaces, lowest peak shear stress was observed for SG-Sand interfaces, which are considerably lesser than the corresponding values of peak shear stress measured in sand alone direct shear tests (Fig. 2). Shear response of triangular geogrid-sand, and hexagonal geogrid-sand interfaces with different surface texture configurations is presented in Figs. 10 and 11, respectively.

Mohr-Coulomb failure envelopes for various square geogrid-sand interfaces are presented in Fig. 12a. The shear strength of the interfaces slightly increased with the provision of pins on the geogrids and

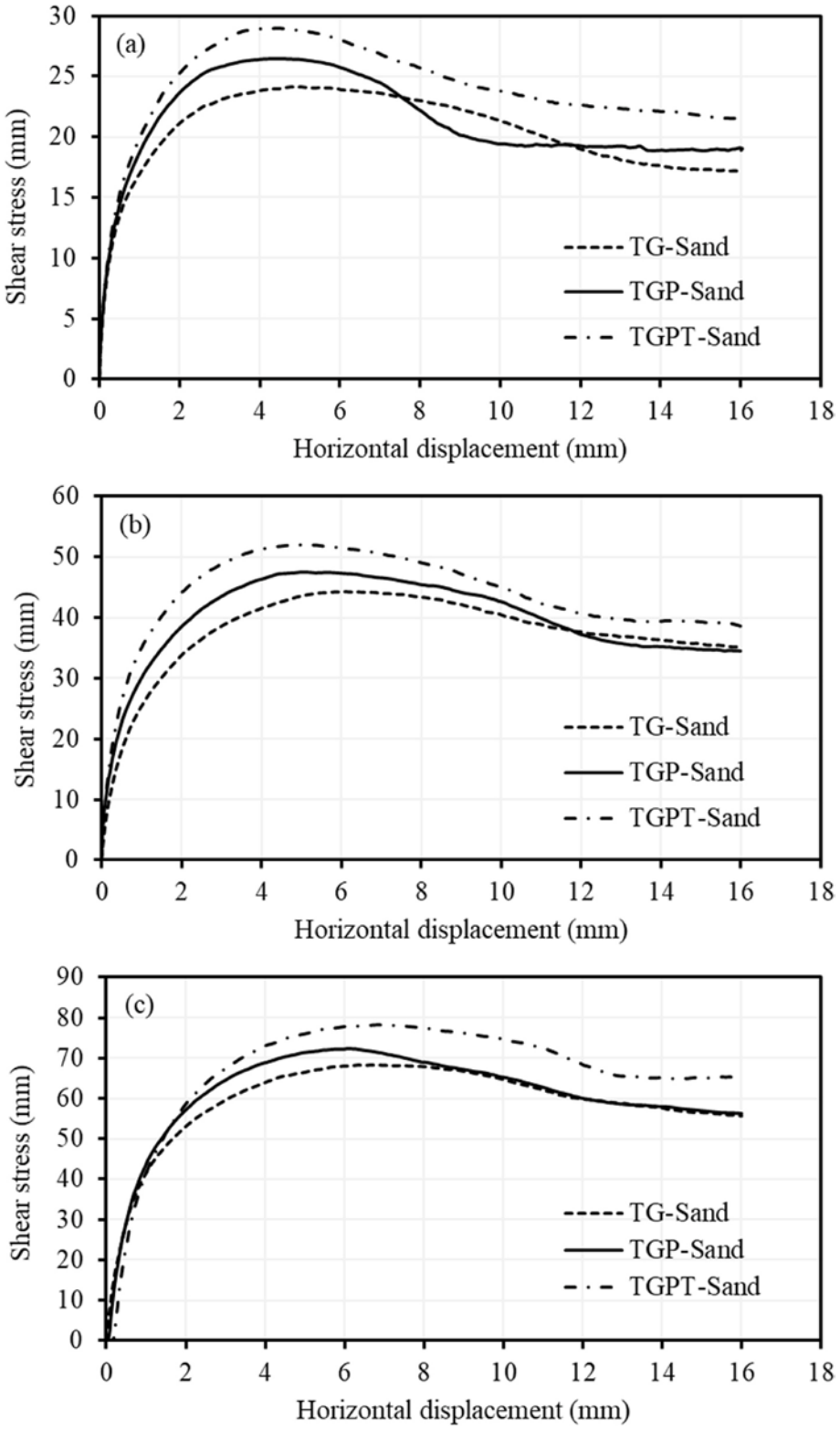

Fig. 10. Shear stress variation of triangular geogrid-sand interface with different texture configurations: (a) 40 kPa; (b) 80 kPa; and (c) 120 kPa.

considerable improvement was seen with the addition of surface texture. The interface friction angle values for SG-Sand and SGP-Sand interfaces were calculated as 26.9°, and 27.6°, respectively. Whereas apparent cohesion was observed as 1.6 kPa for SG-Sand, and 2.93 for SGP-Sand interface condition. These observations demonstrate that the provision of pins at the junction of geogrid (SGP) contributes mainly for improving the apparent cohesion than the interface friction angle. During shearing, when the sand particles move over the geogrids, presence of pins obstructs the movement significantly and results in the accumulation of sand particles near the junctions. This agglomeration effect of pins is the primary reason for the improvement in cohesion with the addition of pins. Further, higher interface friction angle of 29.5° and apparent cohesion of 3.43 kPa were observed for the SGPT-Sand interfaces. The surface texture of 1 mm height in diamond pattern facilitated substantial

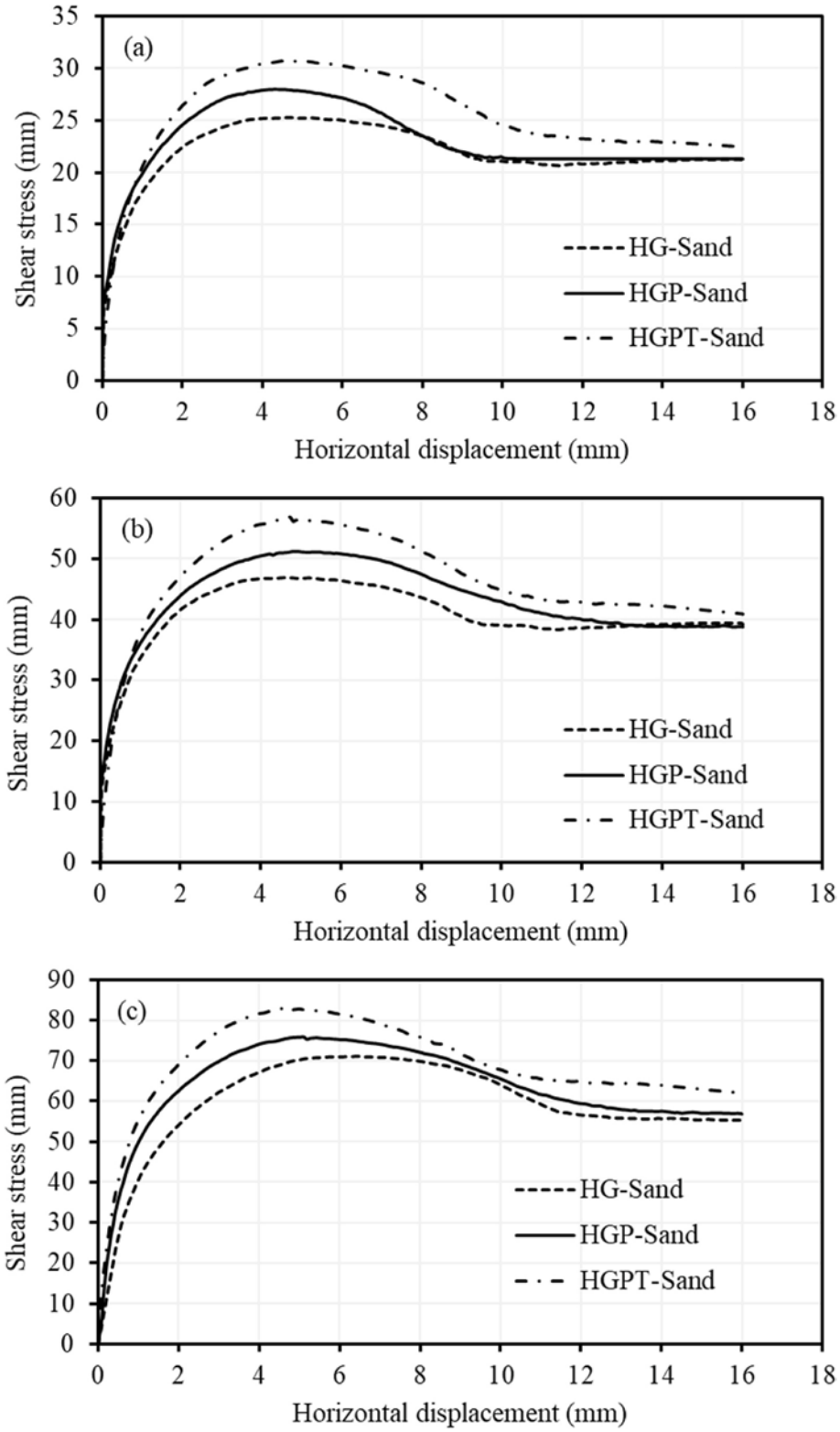

Fig. 11. Shear stress variation of hexagonal geogrid-sand interface with different texture configurations: (a) 40 kPa; (b) 80 kPa; and (c) 120 kPa.

interlocking of sand particles into the texture, thereby increasing both the apparent cohesion and interface friction angle significantly. Also, SGPT has pins, which contribute to the agglomeration effect. Hence, the combination of pins at the junction and texture on the surface of the ribs help in achieving greater interface shear strength of geogrids with minor structural modifications to the geogrids.

The influence of surface texture configuration on the shear strength of different triangular geogrid-sand interfaces and hexagonal geogrid-sand interfaces are shown in Fig. 12b and c, respectively. The friction angles of TG-Sand, TGP-Sand, and TGPT-Sand interfaces were calculated as 28.1°, 29.3°, and 31.4°, respectively. These friction angles are greater than those of the corresponding square geogrid-sand interfaces. In all configurations, hexagonal geogrids exhibited highest interface shear strength compared to triangular and square geogrids. The friction angles

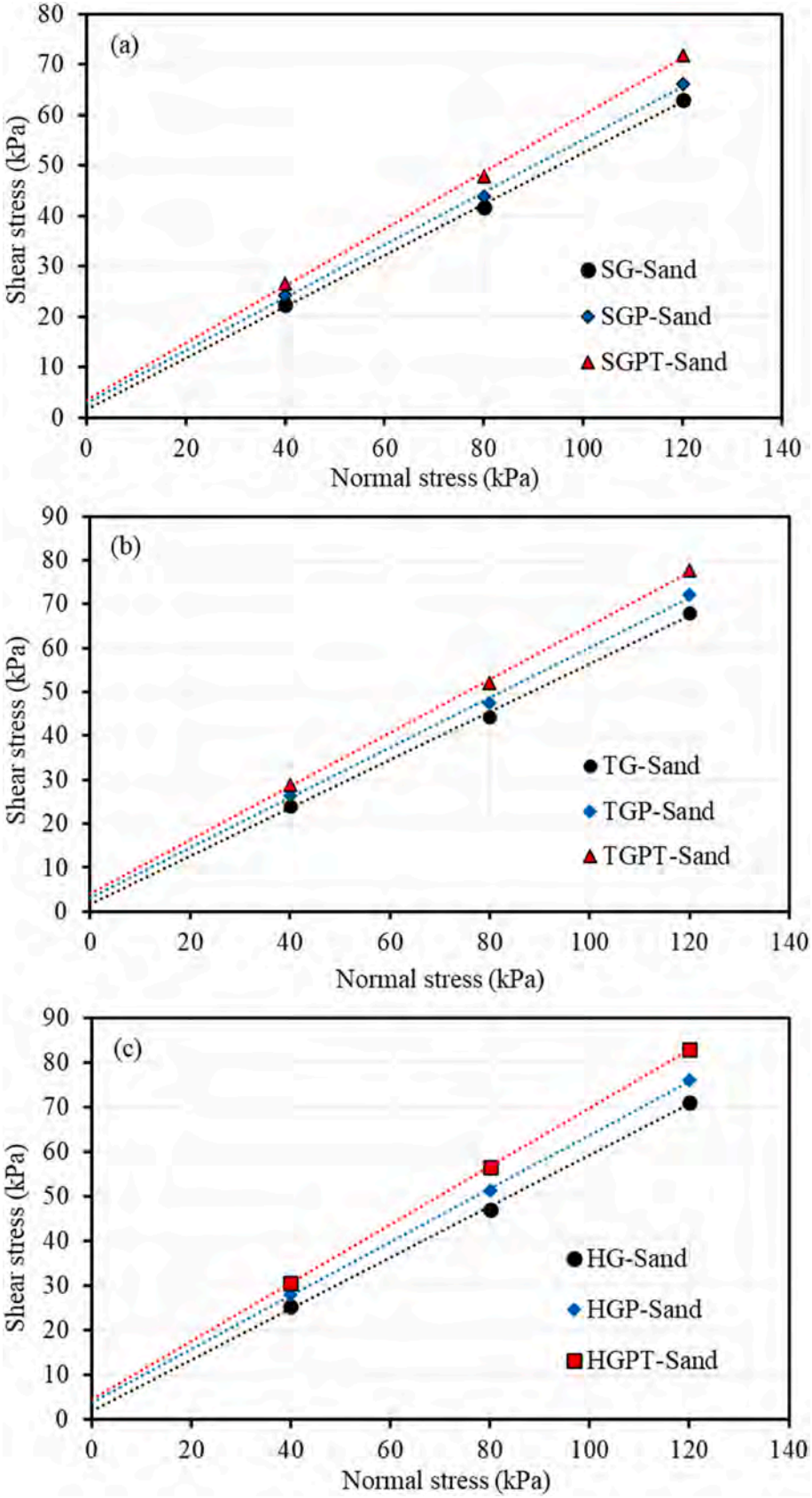

Fig. 12. Failure envelopes for different configurations of geogrid-sand interfaces (a) square geogrids (b) triangular geogrids (c) hexagonal geogrids.

of HG-Sand, HGP-Sand, and HGPT-Sand interfaces are computed as 29.8°, 30.9°, and 33.1°, respectively. The better shear resistance of TG-Sand interfaces in comparison with the SG-Sand interfaces is due to the improvement in passive resistance and rib interference owing to the aperture shape. Diagonal ribs present in the hexagonal geogrids facilitate better confinement to the soil particles within the aperture compared to triangular and square geogrids. As a result, greater resistance against the lateral movement of soil particles is mobilized in these geogrids, which improved the shear resistance significantly.

Further, interface coefficient (α) is computed for different interfaces and compared. The interface coefficient (α) is obtained by dividing the shear strength of geogrid-sand interfaces with the shear strength of sand-sand interface (Vangla and Gali, 2016; Liu et al., 2009). Table 4 summarizes the values of interface coefficient and dilation angle for all the tested geogrid-sand interfaces. The α value was found to be less than 1.0 for all geogrid-sand interfaces, indicating that interface shear strength is higher for sand-sand interactions than sand-polymer interactions. As discussed earlier, the interface efficiency increased from square to triangular to hexagonal geogrids, due to increase in passive resistance and confinement due to the variations in their geometric structures. While the provision of pins enhanced the interface coefficient due to agglomeration effects, surface texture on ribs has resulted in much higher shear efficiency of interfaces due to interlocking effects. Hexagonal geogrids with pins and surface texture (HGPT) showed interface coefficient of 0.96, which is very close to sand-sand interface coefficient. Such high interface coefficients are highly desirable in geogrid reinforced soil structures, to provide higher resistance to pullout failures.

4.1. Interface shear mechanism

Among the two popular planar polymeric reinforcement types, geotextiles interact with soils only through friction whereas geogrids interact with surrounding soils through friction and interlocking. Hence the interaction mechanism with geogrids is relatively a complex phenomenon. The apertures in geogrids are the hollow spaces formed by the geometric alignment of longitudinal and transverse ribs. The shear stress response of geogrid reinforced soil has three components, which include the internal shear resistance mobilized due to the interlocking of soil particles within the apertures (R_i), the passive resistance derived from the transverse ribs of the geogrid (R_p), and the resistance mobilized by the textured ribs to particle movement over them (R_t). Fig. 13 clearly illustrates these three mechanisms. When the rib surface of a geogrid is smooth, the shear resistance offered by the ribs is very low and the overall shear strength is mainly derived from the passive resistance offered by the ribs and the internal shear resistance between the soil particles. Provision of pins helps in increasing the passive resistance. In the case of textured geogrids, all three components of shear contribute to the interface shear strength. The sand particles get trapped inside the surface texture of the ribs (Fig. 14), resulting in sand-to-sand interactions in case of textured geogrids and this leading to mobilization of higher shear resistance. As a result, greater values of interface coefficient were observed in the case of SGPT-sand, TGPT-sand, and HGPT-sand interfaces compared to the SG-sand, TG-sand, and HG-sand interfaces respectively (refer to Table 4).

4.2. Quantifying the contribution of texture (R_t)

To quantify the contribution of surface texture to the shear strength of geogrid-sand interfaces, a new parameter called *surface texture contribution* (STC) is introduced in this study, which denotes the percentage increase in strength of the geogrid by virtue of the surface texture. Surface texture in this context includes both pins and rib surface texture. For geogrids with only pins at the junction and geogrids with pins and surface texture, the values of STC for geogrids with pins (STCP) and for geogrids with pins and texture (STCPT) are obtained using Equations (1) and (2), respectively.

$$\text{STCPT}\ (\%) = \frac{\tau_{PT} - \tau_G}{\tau_G} \times 100 \tag{2}$$

$$\text{STCP}\ (\%) = \frac{\tau_P - \tau_G}{\tau_G} \times 100 \tag{1}$$

where τ_P represents the shear strength of the interface with a geogrid having pins without texture, τ_{PT} represents the shear strength of the interface with the same geogrid with pins and texture, τ_G is the shear strength of the interface with the same geogrid without pins and texture. Fig. 15 shows the influence of normal stress on the variation of STC for different textured geogrid-sand interfaces. The contribution of surface texture to the shear resistance mobilization at the interface decreased with the increase in normal stress. Higher normal stresses led to increased confinement within the sand specimen and altered the interactions between the soil and geogrid layer. This phenomenon can be explained through the relative sizes of the sand particles and surface texture openings. The surface texture has diamond shaped openings of 2.83 mm side and 1 mm height. During shear, sand particles, which are of average size of 0.7 mm, enter the surface texture openings (Fig. 14). At lower normal stresses, the sand particles do not completely be pushed into the openings and hence the shear interactions mainly happen between sand particles on both sides of the shearing plane. Since sand-to-sand friction is higher, this results in higher shear resistance, which is interpreted as the contribution of surface texture. However, with increase in normal stress, the sand particles are pushed into the surface texture and the interactions happen between sand particles at some locations along the shearing plane and between sand and geogrid at other locations, thereby reducing the overall shear resistance. Hence, STC values found to decrease with an increase in the normal stress. Among the different interfaces tested, the maximum value of STC was 21.3% for the HGPT-sand interface followed by 20% in TGPT-sand interface and 18.8% in the SGPT-sand interface. The maximum contribution offered by the hexagonal textured geogrid is majorly due to the presence of a greater number of junction pins. Number of junction pins present on square, triangular and hexagonal shaped geogrids are 4, 3, and 6 respectively, for the grid around a single aperture. Higher number of pins on the hexagonal geogrid increase the agglomeration effect, which results in higher STC value compared to square and triangular geogrids.

Table 4
Interface coefficient and dilation angle measured for different interfaces.

Normal stress (kPa)	Interface coefficient for different interfaces								
	SG-Sand	SGP-Sand	SGPT-Sand	TG-Sand	TGP-Sand	TGPT-Sand	HG-Sand	HGP-Sand	HGPT-Sand
40	0.69	0.73	0.83	0.76	0.79	0.91	0.8	0.83	0.96
80	0.71	0.73	0.82	0.76	0.78	0.90	0.8	0.82	0.96
120	0.7	0.71	0.8	0.75	0.77	0.86	0.79	0.8	0.92
Dilation angle for different interfaces									
40	7.7	7.7	8.2	7.8	8.3	8.9	8.1	8.8	9.9
80	5.8	6.3	7.1	6.1	6.6	7.6	6.4	7.4	8.7
120	3.4	3.7	3.9	3.7	4.0	4.3	4.2	4.5	4.9

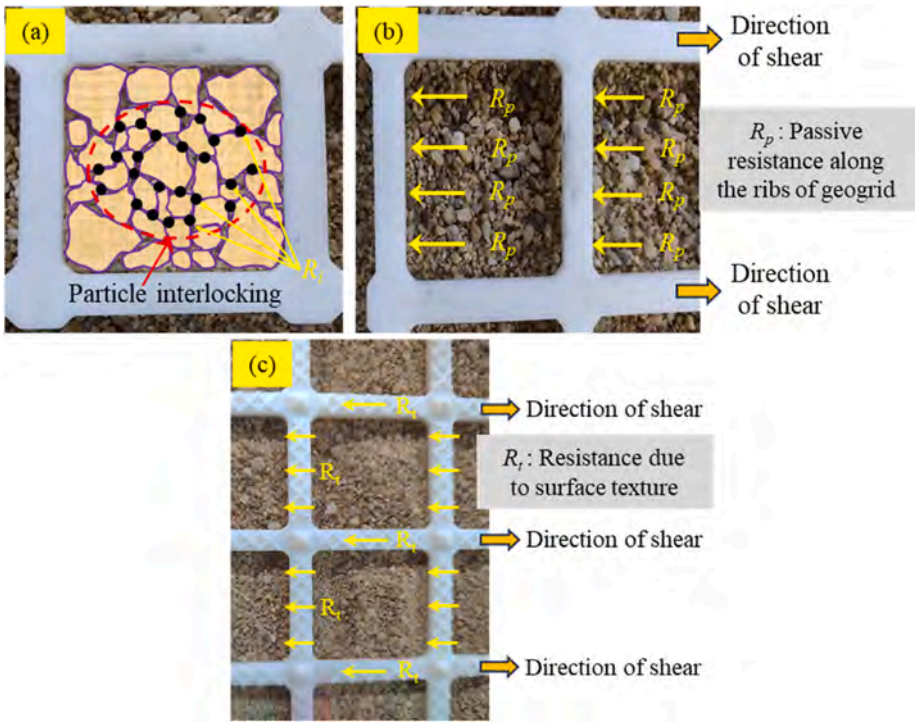

Fig. 13. Distinct aspects of interface mechanism: (a) internal shear resistance mobilized due to the interlocking (R_i); (b) passive resistance from the transverse ribs (R_p); and (c) shear resistance offered by the textured ribs (R_t).

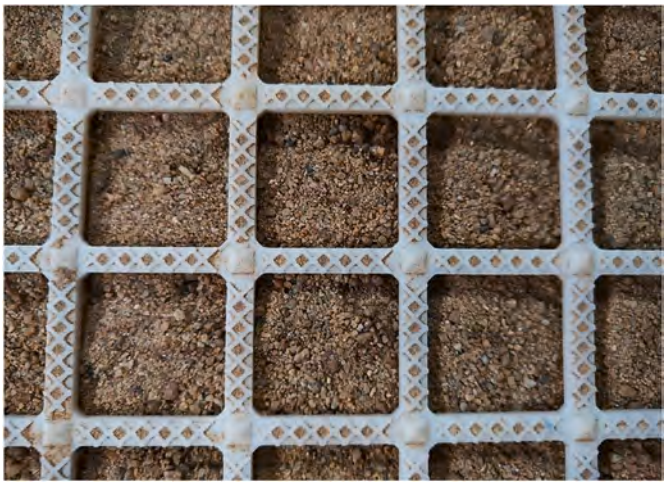

Fig. 14. Particle entrapment in the texture of the geogrid ribs seen after the test.

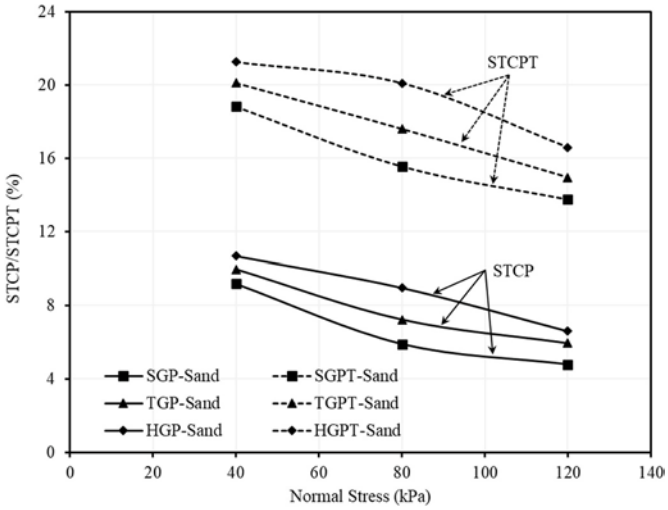

Fig. 15. Contribution of surface texture to the interface shear strength of different geogrid-sand interfaces.

4.3. Dilation angle

In sand-geogrid shear interactions, dilation plays a vital role because it represents the relative vertical movement of particles during horizontal shear, thus defining the overall volumetric deformations in the reinforced soil systems. Hence, it is important to examine the influence of geogrid texture on the dilation angles for the interfaces. The dilation angle (Ψ) is calculated using Equation (3), in which $d(dv)$ is the variation in vertical displacement, and $d(dh)$ is the variation in horizontal displacement (Bolton, 1986; Simoni and Houlsby, 2006).

$$\Psi = \tan^{-1}\left[\frac{d(dv)}{d(dh)}\right] \tag{3}$$

Variation of dilation angle for sand-sand and different geogrid-sand interfaces with the variation in normal stress is shown in Fig. 16. In all the interface tests, dilation angle decreased with the increase in normal stress. The observed variation of dilation angle with the change in normal stress is consistent with the past studies pertaining to the planar geogrid-sand interfaces (Chakraborty and Salgado, 2010; Xiao et al., 2014). Irrespective of geogrid texture, the dilation angle of the different geogrid-sand interfaces was lesser compared to the dilation angle of the sand-sand interfaces because of the confinement effect offered by the geogrids. At lower normal stresses, the geogrids had significant effect in suppressing dilation. However, at a higher normal stress of 120 kPa, the dilation is already restrained by the vertical normal stress and hence the effect of geogrid in reducing the dilation is less pronounced. All textured geogrids exhibited higher dilation angles compared to geogrids without

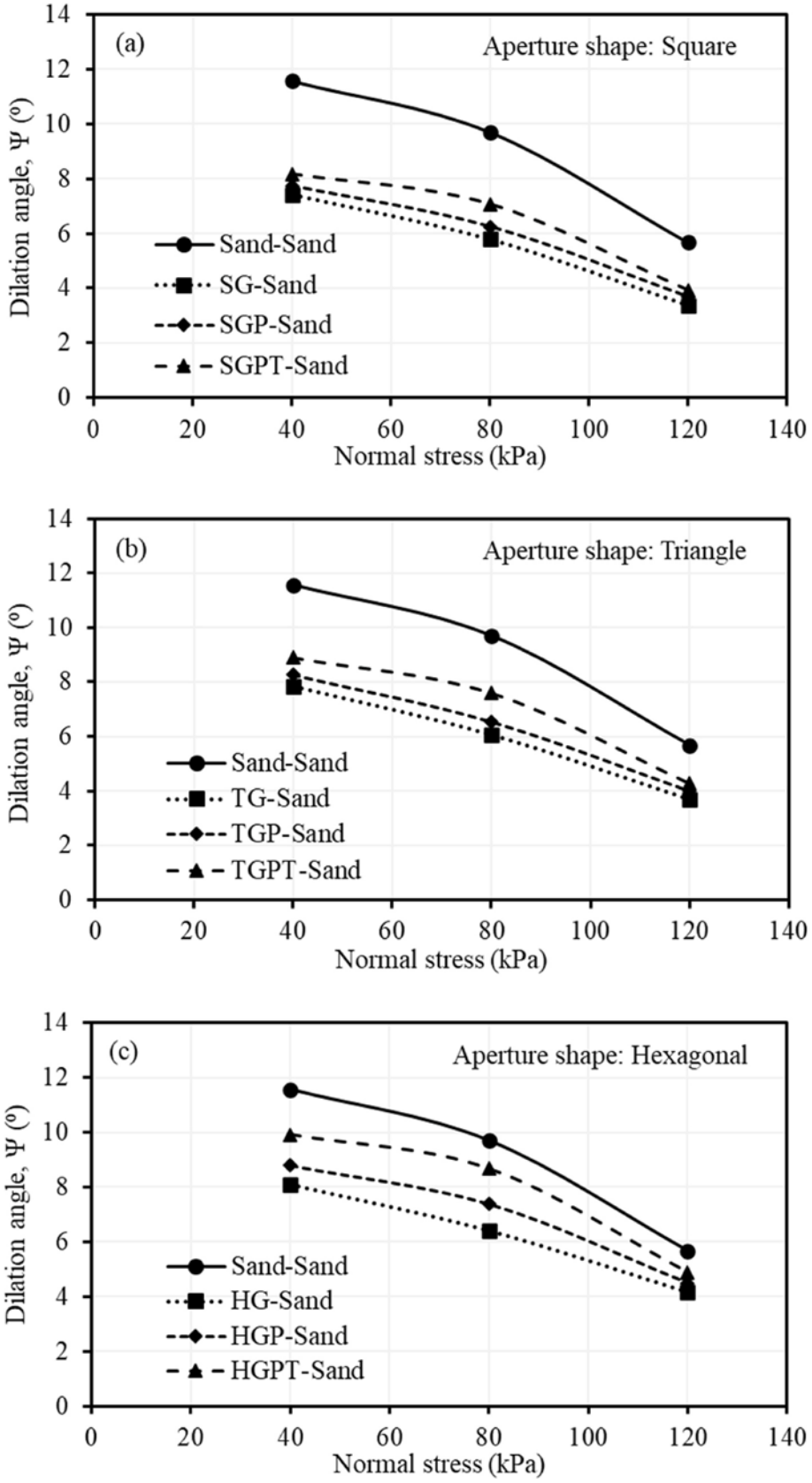

Fig. 16. Variation of dilation angle with normal stress for different configurations of geogrid-sand interfaces: (a) square; (b) triangular; and (c) hexagonal.

texture, irrespective of the aperture shape.

The higher interface shear strength is associated with higher dilation angles for all interface shear tests. The interface coefficient of sand-sand interfaces is 1.0 and it decreased in case of sand-geogrid interfaces and the dilation angle also decreased in the same order, as shown in Table 4. The textured hexagonal geogrid showed maximum dilation followed by the textured triangular geogrid, and the textured square geogrid. The reason for this variation is the higher confinement offered by the hexagonal shape, resulting in lesser vertical deformations for a specific increment in horizontal shear displacement. Moreover, the provision of texture on the rib surface allows the particle entrapment and facilitates the sand-to-sand grain interaction, leading to increase in interlocking effect and dilation behavior. Higher dilation angle in the case of textured hexagonal geogrid-sand interface complements the higher interface shear strength response noticed from the interface direct shear tests. Hence textured geogrids offer better interface shear strength, which is desirable in reinforced soil structures.

4.4. PIV analysis

To visualize and interpret particle dynamics during interface shear tests, PIV analysis was performed for tests with all types of geogrids. The PIV analysis conducted in this study corresponds to the peak shear stress stage of different geogrid-sand interfaces at normal stress of 120 kPa.

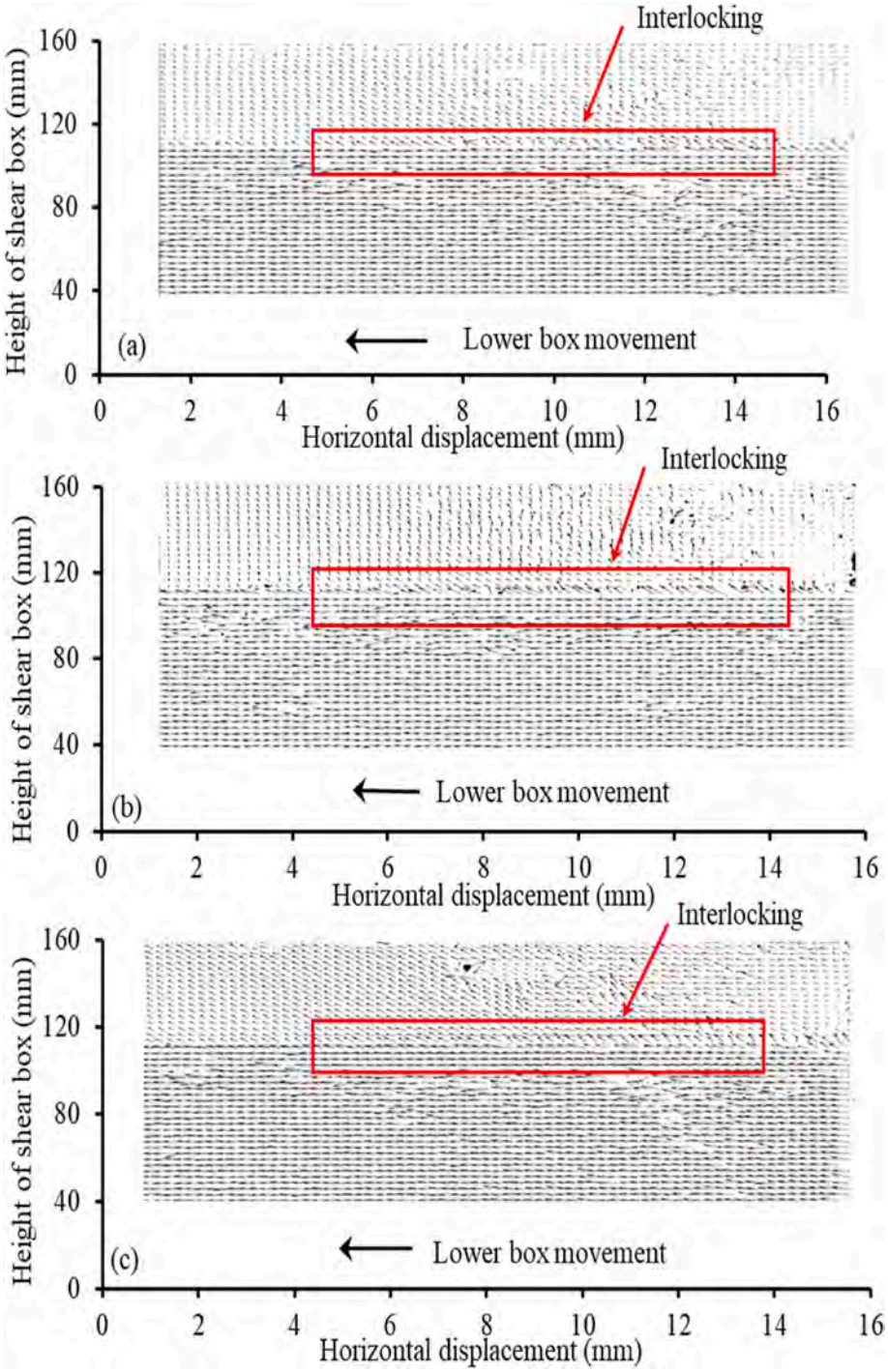

Fig. 17. PIV plots corresponding to peak shear stress of different plain geogrid-sand interfaces: (a) SG-Sand; (b) TG-Sand; and (c) HG-Sand.

PIV analysis is presented for the interface shear tests on plain geogrids and textured geogrids, representing two extreme cases of interface shear resistance, the least in case of the plain geogrid and the highest in case of the textured geogrid. PIV plots correspond to the particle movement of plain geogrid-sand interfaces is shown in Fig. 17. Additionally, shear zone thickness was determined for each geogrid-sand interface from the plots of change in horizontal velocity (aligned with the shear direction) of particles along a vertical section of the shear box was plotted, as shown in Fig. 18. The thickness of the shear zone is computed as the thickness over which the velocity experiences a drop between two stable stages, as marked in Fig. 18. The interlocking effect within the apertures of the geogrid at the interface is observed to increase from square geogrid (Fig. 17a) to triangular geogrid (Fig. 17b) and attained its maximum for hexagonal geogrid (Fig. 17c). The same is translated into increased shear zone thickness for hexagonal geogrid. The measured shear zone thickness for SG-sand, TG-sand, and HG-sand interfaces were 0.92 cm, 1.3 cm, and 1.7 cm, respectively. It is important to note that the increased interlocking and enhanced shear zone thickness can be directly associated with the increased interface shear parameters observed in the interface shear tests, which are in the increasing order for square, triangular and hexagonal geogrids.

Results of interface shear tests indicated that compared to the aperture shape of the geogrids, texture of the geogrids has major influence on the interface shear strength properties. PIV plots for textured geogrid-sand interfaces with different aperture shapes are shown in Fig. 19. These plots highlight the increased particle interactions in case of textured geogrids compared to their counterparts of plain geogrids shown in Fig. 17. HGPT-sand interface showed highest particle interactions among all the interfaces (Fig. 19c). The SGPT-sand interface showed lowest particle interlocking, followed by the TGPT-sand interface. Further, measurement of the thickness of shear zone for different sand-textured geogrid interfaces is shown in Fig. 20. The shear zone

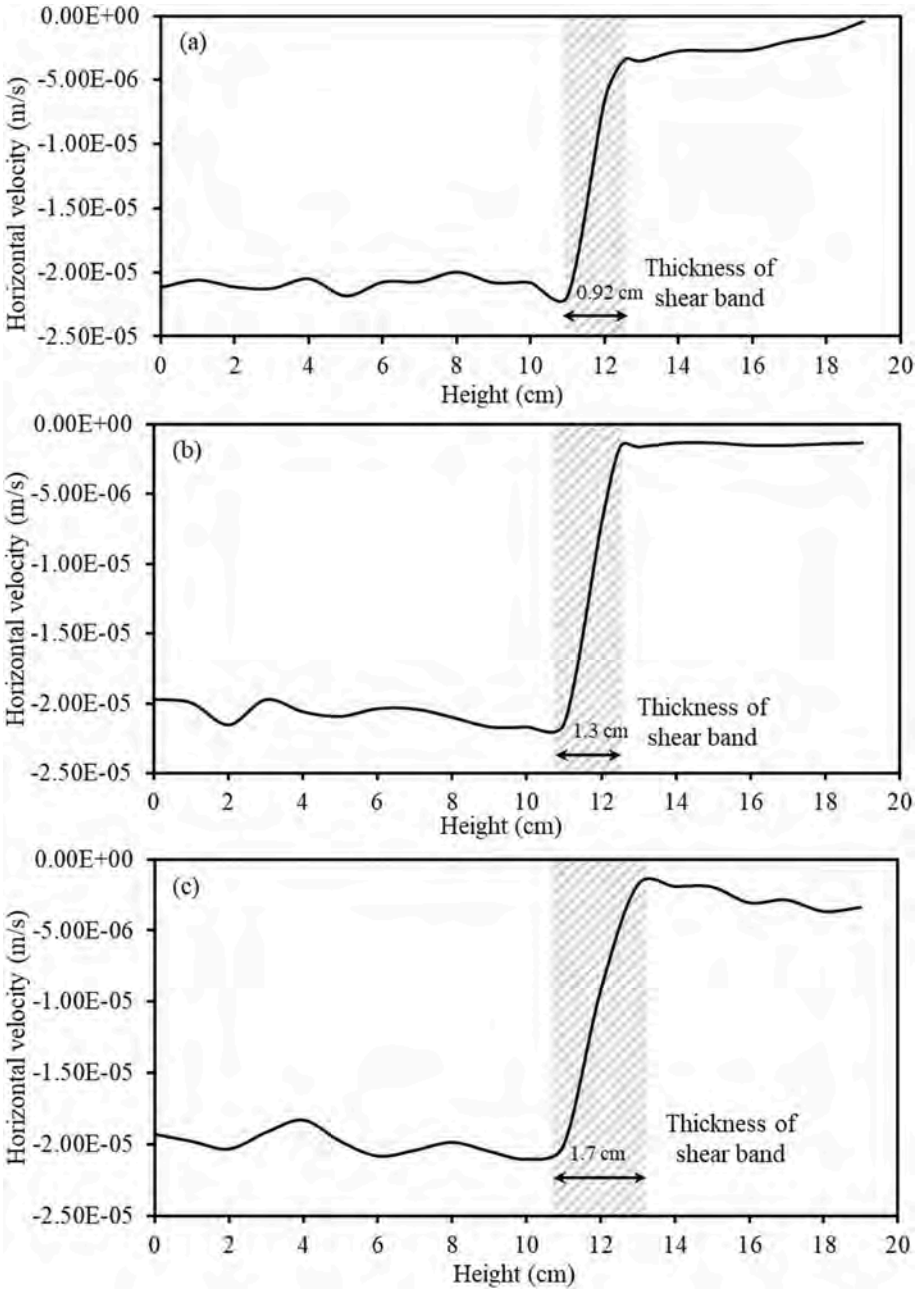

Fig. 18. Variation of shear zone thickness for different plain geogrid-sand interfaces: (a) SG-Sand; (b) TG-Sand; and (c) HG-Sand.

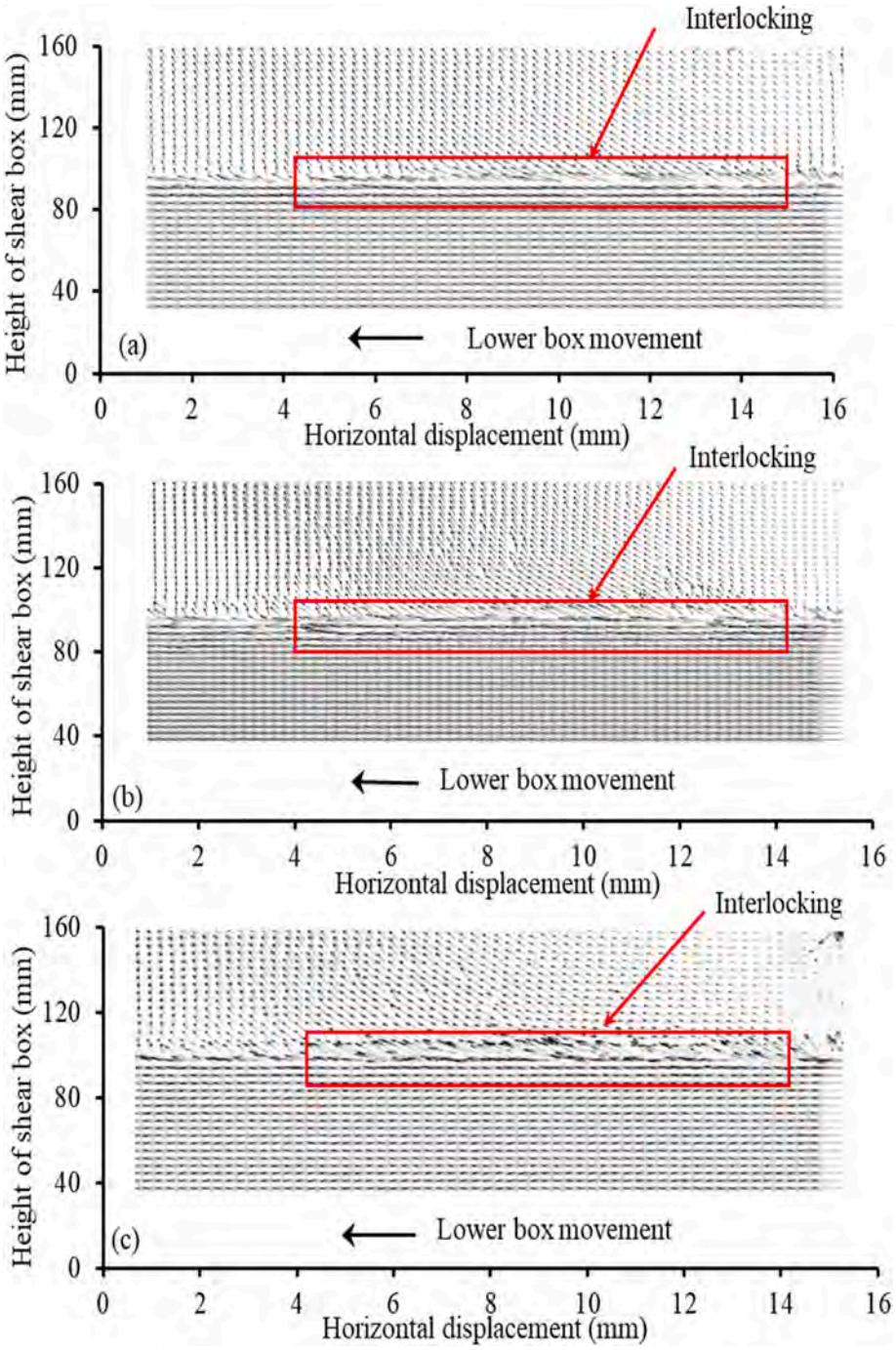

Fig. 19. PIV plots corresponding to peak shear stress of different geogrid-sand interfaces: (a) SGPT-Sand; (b) TGPT-Sand; and (c) HGPT-Sand.

thicknesses for SGPT-sand, TGPT-sand, and HGPT-sand were 1.6 cm, 1.9 cm, and 2.4 cm, respectively. When Figs. 18 and 20 are compared, the shear zone thickness is higher for textured geogrids irrespective of the aperture shape and the difference between the cases of plain geogrids and textured geogrids is significant. In comparison with the SG-sand, TG-sand, and HG-sand interfaces, the thickness of shear zone for SGPT-sand, TGPT-sand, and HGPT-sand interfaces was increased by 25%, 28% and 30%, respectively, Therefore, the provision of surface texture is recommended for achieving the maximum interaction benefits from the geogrid reinforcement.

5. Discussion

The comprehensive investigation with plain and textured geogrids presented in this paper proves that textured geogrids mobilize substantially higher interface shear strength among the tested geogrid shapes. The interface shear strength of geogrids is usually determined through direct shear tests (Chen et al., 2022; Abdi and Safdari Seh Gonbad, 2020), pullout tests (Georgiou et al., 2020; Ye et al., 2022) and inclined plane tests (Bhowmik et al., 2019; Briançon et al., 2011). Among these, direct shear tests and pullout tests are more frequently conducted. In direct shear tests, geogrid is stationery and soil is sheared against the geogrid, whereas in pullout tests, soil is stationery, and the geogrid is pulled out of the soil. Literature suggests that direct shear tests

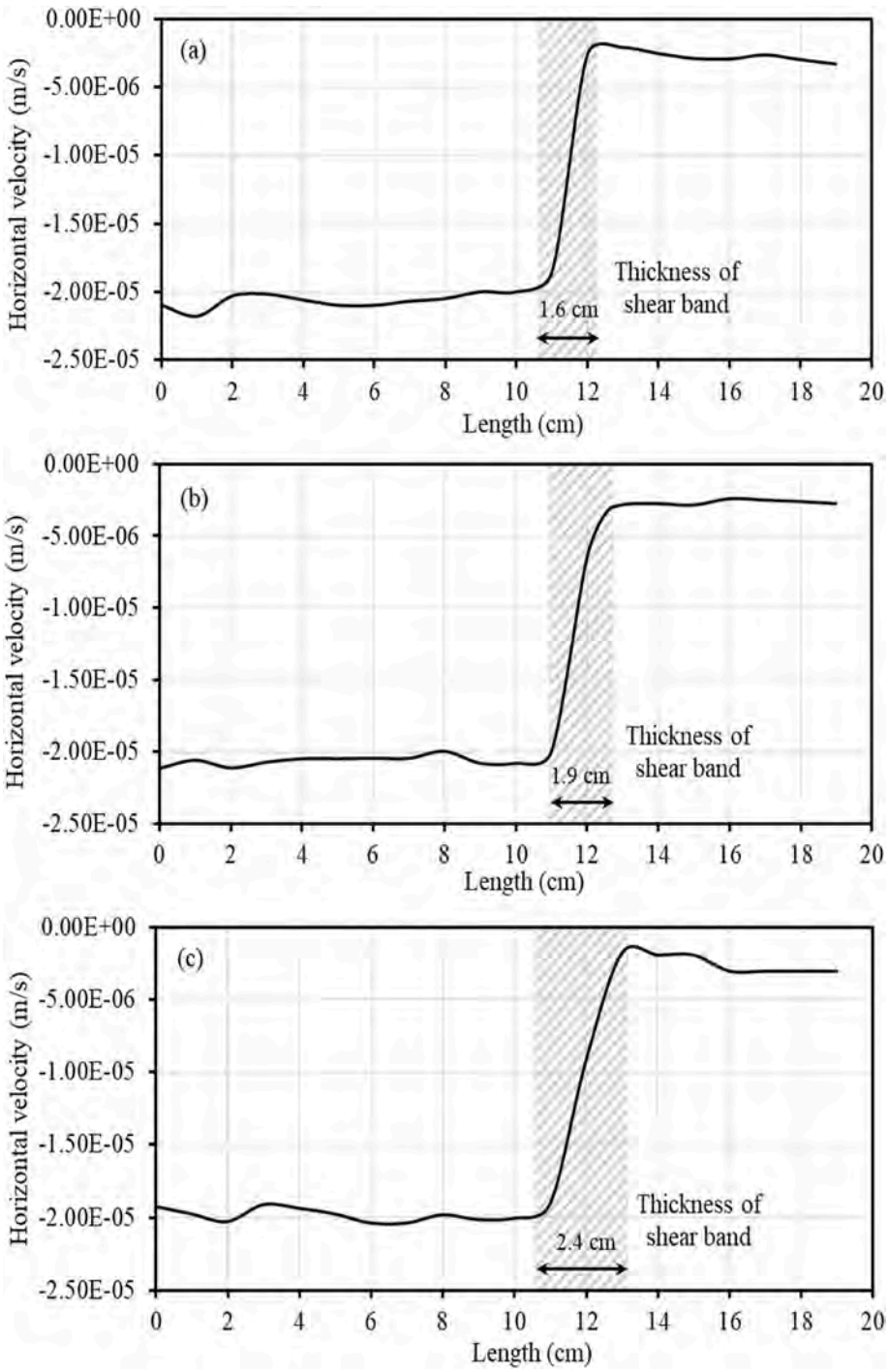

Fig. 20. Variation of shear zone thickness for different geogrid-sand interfaces: (a) SGPT-Sand; (b) TGPT-Sand; and (c) HGPT-Sand.

are more suitable for estimating the interface shear parameters for cases where the strain in the geogrid is minimal and pullout tests are more suitable for cases where geogrids are subjected to significant elongation. Roodi et al. (2018) studied the influence of scaling of the test specimen and the type of test on the load-displacement response, interface shear parameters and displacements measured in direct shear and pullout tests. Results indicated that both the large-scale direct shear and large-scale pullout tests give comparable results and small-scale tests overestimate the geogrid stiffness. In this study, large-scale interface direct shear tests were performed and hence the limitations of small-scale testing and type of test are minimized.

The commercial geogrids which are abundantly being used in numerous reinforced soil structures do not have texture on their surfaces. If the geogrid surface is too smooth, the friction needed to prevent sliding between the geogrid and the surrounding soil or other layers can be compromised, jeopardizing the overall stability of the structure. Rao (2008) reported the lessons for the failure of reinforced retaining wall pertain to pullout failure between soil and reinforcing grids. In this context, the current study proposes innovative and interactive textured geogrids, which provide multi-fold benefits, which include enhanced bond between soil and geogrid, resulting in higher resistance to sliding or pullout and increased stability of the structure.

Though the current study investigated a specific surface texture, many other textures in different geometric proportions and shapes are

possible, which need further investigations. 3D printing used in this study is only a tool to create desired surface texture for lab-scale experiments. The commercial geogrids manufactured at a larger scale can adopt similar texture through suitable modification of the manufacturing process.

6. Conclusions

The current study proposed a new type of geogrids with texture in the form of pins at the junctions and surface texture on the ribs. Based on the studies carried out, the following conclusions are drawn.

- Tensile strength of geogrids varies significantly with the aperture shape. The tensile strength of 3D printed hexagonal geogrids is 1.3 times and 1.17 times superior to that of the square and triangular geogrids, respectively. Adding surface texture on the ribs of the geogrid increased the tensile strength and failure strain, for all shapes.
- Textured geogrids are highly effective in improving the interface shear strength for all types of geogrids because of higher passive resistance, interlocking along the ribs and improved shear resistance due to pins and texture.
- The interface shear strength is highest for textured hexagonal geogrids with an interface coefficient of 0.96, followed by triangular geogrids with an interface coefficient of 0.90 and square geogrids with an interface coefficient of 0.83. The contribution of texture to interface shear strength is 21.3% for hexagonal geogrid interfaces followed by triangular geogrids with 20% and square geogrids with 18.8%. The higher contribution in case of hexagonal geogrids is due to higher number of junction pins for the same aperture area.
- With the addition of texture, the thickness of the shear zone determined from PIV analysis increased by 30%, 28% and 25%, respectively, for hexagonal, triangular, and square geogrid interfaces, which follows the order of interface shear strength.

Funding statement

This study is conducted with funding provided by the ideation research grant of the National Technical Textiles Ministry of India and SERB Core Research Grant CRG/2021/001774 from the Department of Science and Technology (DST), India, and the DRIP research grant of the Department of Civil Engineering, IISc from the Central Water Commission, India.

CRediT authorship contribution statement

Hasthi Venkateswarlu: Writing – review & editing, Writing – original draft, Methodology, Investigation, Formal analysis, Data curation, Conceptualization. **G. Madhavi Latha:** Writing – review & editing, Supervision, Resources.

Declaration of competing interest

The authors declare the following financial interests/personal relationships which may be considered as potential competing interests: Hasthi Venkateswarlu reports was provided by Indian Institute of Science. Hasthi Venkateswarlu reports a relationship with Indian Institute of Science that includes: employment. Hasthi Venkateswarlu has patent pending to Filed. The co-author is currently working as a Professor in the department of Civil Engineering at the Indian Institute of Science Bangalore. If there are other authors, they declare that they have no known competing financial interests or personal relationships that could have appeared to influence the work reported in this paper.

Data availability

Data will be made available on request.

References

Abdi, M.R., Mirzaeifar, H., 2017. Experimental and PIV evaluation of grain size and distribution on soil–geogrid interactions in pullout test. Soils Found. 57 (6), 1045–1058.
Abdi, M.R., Safdari Seh Gonbad, M., 2020. Enhancement of soil–geogrid interactions in direct shear mode using attached elements as anchors. Euro. J. Environ. Civil Eng. 24 (8), 1161–1179.
Arab, M.G., Omar, M., Alotaibi, E., Mostafa, O., Naeem, M., Badr, O., 2020. Bio-inspired 3D-printed honeycomb for soil reinforcement. In: Geo-Congress 2020: Biogeotechnics. American Society of Civil Engineers, Reston, VA, pp. 262–271.
Araújo, G.L.S., Sánchez, N.P., Palmeira, E.M., de Almeida, M.D.G.G., 2022. Influence of micro and macroroughness of geomembrane surfaces on soil-geomembrane and geotextile-geomembrane interface strength. Geotext. Geomembranes 50 (4), 751–763.
Arulrajah, A., Rahman, M.A., Piratheepan, J., Bo, M.W., Imteaz, M.A., 2014. Evaluation of interface shear strength properties of geogrid-reinforced construction and demolition materials using a modified large-scale direct shear testing apparatus. J. Mater. Civ. Eng. 26 (5), 974–982.
ASTM D-2487, 2011. Standard Practice Classification of Soils for Engineering Purposes (Unified Soil Classification System). ASTM International., West Conshohocken, PA, USA.
ASTM D-4253, 2016. Standard Test Methods for Maximum Index Density and Unit Weight of Soils Using a Vibratory Table. ASTM International, Conshohocken, PA, USA.
ASTM D-4254, 2016. Standard Test Methods for Minimum Index Density and Unit Weight of Soils Using a Vibratory Table. ASTM International, Conshohocken, PA, USA.
ASTM D-5321, 2002. Standard Test Method for Determining the Coefficient of Soil and Geosynthetic or Geosynthetic and Geosynthetic Friction by the Direct Shear Mehtod. ASTM International.
ASTM D-6637, 2011. Tensile Properties of Geogrids by the Single or Multi-Rib Tensile Method. ASTM International, West Conshohocken, PA, USA.
Bathurst, R.J., Ezzein, F.M., 2015. Geogrid and soil displacement observations during pullout using a transparent granular soil. Geotech. Test J. 38 (5), 673–685.
Bhowmik, R., Shahu, J.T., Datta, M., 2019. Experimental investigations on inclined pullout behaviour of geogrids anchored in trenches. Geosynth. Int. 26 (5), 515–524.
Bolton, M., 1986. The strength and dilatancy of sands. Geotechnique 36 (1), 65–78.
Briançon, L., Girard, H., Gourc, J.P., 2011. A new procedure for measuring geosynthetic friction with an inclined plane. Geotext. Geomembranes 29 (5), 472–482.
Brown, S.F., Kwan, J., Thom, N.H., 2007. Identifying the key parameters that influence geogrid reinforcement of railway ballast. Geotext. Geomembranes 25 (6), 326–335.
Chakraborty, T., Salgado, R., 2010. Dilatancy and shear strength of sand at low confining pressures. Journal of geotechnical and geoenvironmental engineering 136 (3), 527–532.
Chalmovsky, J., Koudela, P., Mica, L., 2020. Reinforcing of sand with 3D printed fibres–review of properties, fabrication of fibres and initial testing programme. In: IOP Conference Series: Materials Science and Engineering, vol. 960. IOP Publishing, 032027, 3.
Chen, J.N., Ren, X., Xu, H., Zhang, C., Xia, L., 2022. Effects of grain size and moisture content on the strength of geogrid-reinforced sand in direct shear mode. Int. J. GeoMech. 22 (4), 04022006.
Derksen, J., Ziegler, M., Fuentes, R., 2021. Geogrid-soil interaction: a new conceptual model and testing apparatus. Geotext. Geomembranes 49 (5), 1393–1406.
Ding, X.M., Luo, Z.G., Ou, Q., 2022. Mechanical property and deformation behavior of geogrid reinforced calcareous sand. Geotext. Geomembranes 50 (4), 618–631.
Dong, Y.L., Han, J., Bai, X.H., 2011. Numerical analysis of tensile behavior of geogrids with rectangular and triangular apertures. Geotext. Geomembranes 29 (2), 83–91.
Escobar, A., Caicedo, B., Cabrera, M., 2021. Interaction between a cylinder and a partially saturated soil for compaction analysis. Transportation Geotechnics 30, 100600.
Ferreira, F.B., Vieira, C.S., Lopes, M., 2015. Direct shear behaviour of residual soil–geosynthetic interfaces–influence of soil moisture content, soil density and geosynthetic type. Geosynth. Int. 22 (3), 257–272.
Ferreira, J.A., Zornberg, J.G., 2015. A transparent pullout testing device for 3D evaluation of soil–geogrid interaction. Geotech. Test J. 38 (5), 686–707.
Fowmes, G.J., Dixon, N., Fu, L., Zaharescu, C.A., 2017. Rapid prototyping of geosynthetic interfaces: investigation of peak strength using direct shear tests. Geotext. Geomembranes 45 (6), 674–687.
Fukuoka, H., Sassa, K., Wang, G., 2007. Influence of shear speed and normal stress on the shear behavior and shear zone structure of granular materials in naturally drained ring shear tests. Landslides 4 (1), 63–74.
Georgiou, I., Loli, M., Kourkoulis, R., Gazetas, G., 2020. Pullout of steel grids in dense sand: experiments and design insights. J. Geotech. Geoenviron. Eng. 146 (10), 04020102.
Giang, N.H., Kuwano, J., Izawa, J., Tachibana, S., 2010. Influence of unloading–reloading processes on the pullout resistance of geogrid. Geosynth. Int. 17 (4), 242–249.

Górszczyk, J., Malicki, K., 2023. New approach to junction efficiency analysis of hexagonal geogrid using digital image correlation method. Geotext. Geomembranes 51 (5), 70–80.
Grognet, M., 2011. The Boundary Conditions in Direct Simple Shear Tests: Developments for Peat Testing at Low Normal Stress. Master's thesis. TU Delft, Delft, The Netherlands.
Jayalath, C., Gallage, C., 2021. Evaluating the tensile properties of geogrids using the particle image Velocimetry technique. J. Mater. Civ. Eng. 33 (11), 04021328.
Koerner, R.M., 2000. Emerging and future developments of selected geosynthetic applications. J. Geotech. Geoenviron. Eng. 126 (4), 293–306.
Lashkari, A., Jamali, V., 2021. Global and local sand–geosynthetic interface behaviour. Geotechnique 71 (4), 346–367.
Latha, G.M., Venkateswarlu, H., Krishnaraj, P., Allam, S.K., Anusree, K.V., Krishna, A., 2024. Science and technology of additive manufacturing applied to geotechnical engineering. Indian Geotech. J. 54 (1), 85–95.
Liu, C.N., Zornberg, J.G., Chen, T.C., Ho, Y.H., Lin, B.H., 2009. Behavior of geogrid-sand interface in direct shear mode. J. Geotech. Geoenviron. Eng. 135 (12), 1863.
Liu, F.Y., Fu, J., Wang, J., Gao, Z.Y., Li, H.Z., Li, J.T., 2022. Effect of the particle size ratio on macro-and mesoscopic shear characteristics of the geogrid-reinforced rubber and sand mixture interface. Geotext. Geomembranes 50 (4), 779–793.
Liu, S., Huang, H., Qiu, T., Kwon, J., 2016. Effect of geogrid on railroad ballast particle movement. Transportation Geotechnics 9, 110–122.
Liu, 2020. Spider web inspired geogrid for geotechnical applications and future developments of selected geosynthetic applications. Center for Bio-Mediated and Bio-Inspired Geotechnics (CBBG) YR5 Poster Session, Wednesday, October 28th, 2020. Arizona State University, USA.
Maghool, F., Arulrajah, A., Mirzababaei, M., Suksiripattanapong, C., Horpibulsuk, S., 2020. Interface shear strength properties of geogrid-reinforced steel slags using a large-scale direct shear testing apparatus. Geotext. Geomembranes 48 (5), 625–633.
Makkar, F.M., Chandrakaran, S., Sankar, N., 2019. Experimental investigation of response of different granular soil–3D geogrid interfaces using large-scale direct shear tests. J. Mater. Civ. Eng. 31 (4), 04019012.
Mirzaalimohammadi, A., Ghazavi, M., Lajevardi, S.H., Roustaei, M., 2019. Laboratory studies of interaction properties between fine sand and various grid reinforcements. Innovative Infrastructure Solutions 4, 1–13.
Mishra, S.R., Nithin, S., Mohapatra, S.R., Rajagopal, K., 2016. Application of image processing technique in wide width tensile testing of nonwoven geotextile. In: Sixth Asian Regional Conference on Geosynthetics. International Geosynthetics Society, Jupiter, FL, New Delhi, India, pp. 795–803.
Miyata, Y., Bathurst, R.J., 2012. Reliability analysis of soil-geogrid pullout models in Japan. Soils Found. 52 (4), 620–633.
Mosallanezhad, M., Alfaro, M.C., Hataf, N., Taghavi, S.S., 2016. Performance of the new reinforcement system in the increase of shear strength of typical geogrid interface with soil. Geotext. Geomembranes 44 (3), 457–462.
Naeini, S.A., Khalaj, M., Izadi, E., 2013. Interfacial shear strength of silty sand–geogrid composite. Proceedings of the Institution of Civil Engineers-Geotechnical Engineering 166 (1), 67–75.
Palmeira, Ennio M., Antunes, Luiz G.S., 2010. Large scale tests on geosynthetic reinforced unpaved roads subjected to surface maintenance. Geotext. Geomembranes 28 (6), 547–558.
Peerun, M.I., Ong, D.E.L., Choo, C.S., 2019. Interpretation of geomaterial behavior during shearing aided by PIV technology. J. Mater. Civ. Eng. 31 (9), 04019195.
Pitanga, H.N., Gourc, J.P., Vilar, O.M., 2009. Interface shear strength of geosynthetics: evaluation and analysis of inclined plane tests. Geotext. Geomembranes 27 (6), 435–446.
Prakash, K.K., Rathod, D., Muthukkumaran, K., 2023. Role of Geogrid reinforcement and its diverse applications in the geotechnical engineering and allied fields: a-state-of-the-art review. Aust. J. Civ. Eng. 1–19.
Rao, P.J., 2008. Practical lessons from failure of a reinforced soil retaining wall on a major highway. Sixth International Conference on Case Histories in Geotechnical Engineering, Arlington, VA, August 11-16,, 2008.
Razeghi, H.R., Ensani, A., 2023. Clayey sand soil interactions with geogrids and geotextiles using large-scale direct shear tests. International Journal of Geosynthetics and Ground Engineering 9 (2), 24.
Roodi, G.H., Morsy, A.M., Zornberg, J.G., 2018. A Study on the effect of scale and testing method on soil-geosynthetic interaction. In: Proceedings of the 11th International Conference on Geosynthetics, 16–21 September 2018, Seoul, Republic of Korea.
Shukla, S.K., 2004. Discussion: applications of geosynthetics for soil reinforcement. Proceedings of the Institution of Civil Engineers-Ground Improvement 8 (4), 179–182.
Simoni, A., Houlsby, G.T., 2006. The direct shear strength and dilatancy of sand–gravel mixtures. Geotech. Geol. Eng. 24, 523–549.
Stanier, S.A., Blaber, J., Take, W.A., White, D.J., 2016. Improved image-based deformation measurement for geotechnical applications. Can. Geotech. J. 53 (5), 727–739.
Stathas, D., Wang, J.P., Ling, H.I., 2017. Model geogrids and 3D printing. Geotext. Geomembranes 45 (6), 688–696.
Stoltz, G., Nicaise, S., Veylon, G., Poulain, D., 2020. Determination of geomembrane–protective geotextile friction angle: an insight into the shear rate effect. Geotext. Geomembranes 48 (2), 176–189.
Vangla, P., Gali, M.L., 2016. Effect of particle size of sand and surface asperities of reinforcement on their interface shear behaviour. Geotext. Geomembranes 44 (3), 254–268.
Venkateswarlu, H., Hegde, A., 2019. Block resonance test on geosynthetic reinforced foundation beds. In: Meehan, C.L., Kumar, S., Pando, M.A., Coe, J.T. (Eds.), Geo-congress 2019: Earth Retaining Structures and Geosynthetics. American Society of Civil Engineers, Reston, pp. 266–276.
Venkateswarlu, H., Krishnaraj, P., Latha, G.M., 2023a. Three-dimensionally printed polypropylene sheets: insights on mechanical and interface shear behavior. J. Mater. Civ. Eng. 35 (9), 04023284.
Venkateswarlu, H., SaiKumar, A., Latha, G.M., 2023b. Sand-geogrid interfacial shear response revisited through additive manufacturing. Geotext. Geomembranes 51 (4), 95–107.
Vieira, C.S., Pereira, P.M., 2016. Interface shear properties of geosynthetics and construction and demolition waste from large-scale direct shear tests. Geosynth. Int. 23 (1), 62–70.
White, D.J., Take, W., Bolton, M., 2003. Soil deformation measurement using Particle Image Velocimetry (PIV) and photogrammetry. Geotechnique 53 (7), 619–631.
White, D., Take, A., 2002. GeoPIV: Particle Image Velocimetry (PIV) Software for Use in Geotechnical Testing. CUED/D-SOILS/TR322, Cambridge, UK.
Wu, Z.J., Zhang, B., Weng, L., Liu, Q.S., Wong, L.N.Y., 2020. A new way to replicate the highly stressed soft rock: 3D printing exploration. Rock Mech. Rock Eng. 53 (1), 467–476.
Xiao, Y., Liu, H., Chen, Y., Chu, J., 2014. Influence of intermediate principal stress on the strength and dilatancy behavior of rockfill material. J. Geotech. Geoenviron. Eng. 140 (11), 04014064.
Ye, Y., Han, J., Liu, H., Rachford, S.M., Parsons, R.L., Dolton, B., O'Reilly, M., 2022. Pullout resistance of geogrid and steel reinforcement embedded in lightweight cellular concrete backfill. Geotext. Geomembranes 50 (3), 432–443.
Ying, M., Liu, F., Wang, J., Wang, C., Li, M., 2021. Coupling effects of particle shape and cyclic shear history on shear properties of coarse-grained soil–geogrid interface. Transportation Geotechnics 27, 100504.
Zeng, W.X., Liu, F.Y., Zhu, X.X., He, J.H., Wang, J., 2022. Discrete element method investigation of shear behaviour of 3D geogrid–sand interface. Geosynth. Int. 1–11.
Zhang, J., Cao, W.Z., Zhou, Y.J., 2021a. Mechanical behavior of triaxial geogrid used for reinforced soil structures. Adv. Civ. Eng. 2021 (1), 5598987.
Zhang, J., Ji, M., Jia, Y., Miao, C., Wang, C., Zhao, Z., Zheng, Y., 2021b. Anisotropic shear strength behavior of soil–geogrid interfaces. Appl. Sci. 11 (23), 11387.
Zhou, J., Chen, J.F., Xue, J.F., Wang, J.Q., 2012. Micro-mechanism of the interaction between sand and geogrid transverse ribs. Geosynth. Int. 19 (6), 426–437.
Ziegler, M., 2017. Application of geogrid reinforced constructions: history, recent and future developments. Procedia Eng. 172, 42–51.